Chapter

MODEL PREDICTIVE CONTROL OF LARGE SCALE SOLAR TROUGH PLANTS

Eduardo F. Camacho*, Adolfo J. Sánchez and Antonio J. Gallego

Departamento de Ingeniería de Sistemas y Automática,
Universidad de Sevilla, Sevilla, Spain

ABSTRACT

One of the current technological challenges is to make solar energy economical and competitive. Advanced control techniques may contribute in this direction by maximizing the electricity generated by using optimal control strategies.

A number of research works have been developed concerning control and optimization of solar plants. Most of these works have been developed for the experimental solar trough plant of ACUREX at the Plataforma solar de Almería (PSA) (10 parallel loops of collectors). Generally, small plants such as the ACUREX field can be modelled as an equivalent loop for developing control strategies. Commercial solar trough plants are very extensive, covering vast areas. As an example, Solana Generating Station which has 808 parallel loops of four collectors connected in series (3,232

* Corresponding Author address. Email: efcamacho@us.es.

collectors) covering 780 hectares. The optimization of large scale solar trough plants poses important challenges which require new advanced control techniques to address them:

1. The optical efficiency of different groups of loops may be substantially different in large scale solar plants. The most efficient loops will probably have to be defocused to avoid excessive temperatures. Paradoxically, the most efficient loops will have the higher energy losses because of defocusing. To avoid this energy loss, the valves of the most efficient loops would have to be opened to increase the HTF flow. However, any movement of the valve in one of the loops will influence the flow of the rest of the loops. Loop valves are only used in current plants for steady state flow balancing.
2. Scattered clouds may only affect the locations where the sensors are placed, while the rest of the plant may be under the effect of intense DNI, or vice versa. Sudden changes in DNI produced by scattered clouds induce oscillations so severe that the solar field may have to be defocused or shutdown. This fact produces, in general, not only energy losses but plant deterioration. A spatially distributed DNI nowcasting can be used to improve plant operation and optimize the production.

This chapter presents some new concepts and ideas that the authors believe will be the future steps in the development and progress of solar thermal energy. Preliminary results for advanced control of solar plants are presented, using more effective defocusing mechanisms and dynamic thermal balance of loops that have already shown to produce significant gains,.

Keywords: solar parabolic, model predictive control, collector defocus, electric power limitation, large scale

NOMENCLATURE

A	Cross-sectional area of the pipe (m^2)
$C(t,T)$	Specific heat capacity ($\mathrm{J}/(\mathrm{kg}^\circ\mathrm{C})$)
D	Hydraulic diameter of the pipe (m)
G	Collector aperture (m)

$H_l(t,T)$	Thermal loss global coefficient ($\mathrm{W}/(\mathrm{m}^2\mathrm{C})$)
$H_t(t,T,q)$	Metal-fluid heat transmission coefficient
$I(t)$	Direct solar radiation (W/m^2)
$k(t,T)$	Thermal conductivity ($\mathrm{W}/(\mathrm{m}^\circ\mathrm{C})$)
K_{opt}	Optical efficiency (Unitless)
L	Length of pipeline (m)
$n_o(t)$	Geometric efficiency (Unitless)
Nu	Nusselt number
P	Power (MW)
PW_{ref}	Reference to the Power GS-GPC
$PW_{set-point}$	Power set-point by TSO
PW_{TSO}	Boolean variable indicating the plant is on limitation mode
TSO_L	Boolean variable indicating the plant received a power limitation
P_{cp}	Fixed factor (loop geometrical and thermal properties)
phi	Fixed factor (Unitless)
Pr	Prandtl number
$q(t)$	Loop oil flow rate (m^3/s)
$Q(t)$	Solar field oil flow rate ($\mathrm{m}^3/\mathrm{h}, \mathrm{kg}/\mathrm{s}$)
q_{ff}	Computed flow-rate by the Feed Forward (1 Loop) (m^3/s)
Q_{ff}	Computed flow-rate by the Feed Forward (N Loops) (m^3/s)
Q_{high}	Flow limit to consider the plant is saturated
Q_{low}	Flow limit to consider the plant is not saturated
Q_{PW}	Power GS-GPC Flow-rate (m^3/s)
Re	Reynolds number
S	Total reflective surface (m^2)
t	Time (s)
$T(x,t)$	Temperature ($^\circ\mathrm{C}$)
$T_a(t)$	Ambient temperature ($^\circ\mathrm{C}$)
T_{in}	Inlet temperature ($^\circ\mathrm{C}$)

T_{out}	Outlet temperature ($^{\circ}$C)
T_{mean}	Mean temperature between inlet and outlet temperature ($^{\circ}$C)
$T_{set-point}$	Temperature reference for tracking ($^{\circ}$C)
T_{high}	Field outlet temperature to consider the plant is saturated
T_{low}	Field outlet temperature to consider the plant is not saturated
T_{C3}^{i}	Third collector temperature (loop i) ($^{\circ}$C)
T_{ref-C3}	Temperature set-point applied to the 3^{rd}collector ($^{\circ}$C)
T_{ref-C4}	Temperature set-point applied to the 4^{th}collector ($^{\circ}$C)
$T_{ref-sat}$	Temperature set-point for 4^{th} collector in saturation ($^{\circ}$C)
$T_{ref-nosat}$	Temperature set-point for 4^{th} collector not in saturation ($^{\circ}$C)
x	Space (m)
ΔT	Thermal difference ($^{\circ}$C)
β_k^i	Defocus angle, 4^{th} collector, loop i, instant k (deg)
γ_k^i	Defocus angle, 3^{th} collector, loop i, instant k (deg)
$\mu(t,T)$	Dynamic viscosity of the fluid (Pa · s)
$\nu(t,T)$	Kinematic viscosity (m^2/s)
$\rho(t,T)$	Density (kg/m^3)
η_{ext}	Efficiency considering other effects (Unitless)
η_{par}	Parasitics efficiency (Unitless)
η_{rank}	Rankine cycle efficiency (Unitless)

1. INTRODUCTION

The pressing need to reduce the impact of fossil fuels has increased the interest in tapping renewable energy sources. In particular, the use of solar energy has experienced a great impulse during the last two decades [1]. Governments are promoting the construction and exploitation of solar

energy power plants around the world as a way of overcoming the drawback of producing energy using exhaustible energy sources [2].

During the last 20 years an important number of commercial solar power plants have been commissioned. For example, we can mention the two 50 MW Solacor I and II (in Córdoba (Spain)), and the two 50 MW Helios parabolic trough plants in Castilla la Mancha (Spain) [3]. The 50 MW solar trough plants Andasol I, II and III owned by Cobra/ACS group were constructed in Guadix (Southern Spain) [4]. In the USA we can mention Solana and Mojave Solar parabolic trough plants constructed and operating in Arizona and California respectively [5, 6], each of 280 MW electrical power production. Regarding solar power towers, we can mention PS10 (10 MW), PS20 (20 MW) and Khi Solar owned by Atlantica Yield and Abengoa Solar respectively.

One of the great challenges of this century, identified by the US National Academy of Engineering and the European Commission, is to make solar energy economical and competitive [7, 8]. The application of advanced control and optimization algorithms can play an important role in increasing the overall efficiency of the solar energy plants and thus improve the penetration of this kind of plants into the global market [9].

Most of the research and the application of advanced control techniques have been carried out using the experimental ACUREX solar trough plant at the Solar Platform of Almeria (PSA) as a testbench [10]. For example, in [11, 12] a review of some control strategies applied to the ACUREX solar field is presented. In [13], adaptative control and nonlinear schemes are described for the ACUREX solar field. In [14] a nonlinear neural predictive controller is developed and tested at the real ACUREX plant. In [15], a review of the application of linear and nonlinear model predictive control algorithms to the ACUREX plant is presented. However, there is a lack of experimental research applied to commercial solar trough plants.

Current commercial solar trough plants cover vast extensions of land. The two solar trough plants of Mojave cover 700 hectares and they are composed of 282 loops each [16]. The SOLANA solar trough plant is even larger. It is composed of 808 loops covering 780 hectares [6]. These large-scale solar plants highlight new challenges for the application of advanced

control strategies. New advanced control techniques have to be devised and developed to address these issues.

In order to develop new advanced control strategies for large scale solar plants, the Advanced Grant "Optimal Control of solar energy systems" (OCONTSOLAR) funded by the European Research Council, is being conducted. One of the main objectives of this project is to develop radically new model predictive control (MPC) algorithms which use mobile solar sensors to obtain estimations and predictions of solar radiation mapping [17]. In general, control strategies proposed in the literature use direct solar radiation provided by pyrheliometers. They consider this measurement to be the same for the whole solar field. If the solar field is small, as in the case of the ACUREX field, this assumption can be considered reasonable, but in large scale plants different levels of solar radiation affect the solar field due to passing clouds. Furthermore, the efficiency of the loops can be substantially different when a group of them has been cleaned and others have not [18]. The most efficient loops have to be defocused to avoid excessive temperatures. Paradoxically, the most efficient loops will have the higher energy losses. To avoid this energy loss, the valves of the most efficient loops would have to be opened to increase the HTF flow. However, any movement of the valve in one of the loops will influence the flow of the rest of the loops. Loop valves are only used in current plants for steady state flow balancing.

A preliminary work has been recently published using a model of the ACUREX field [19] as a test-bench. In this work, the input valves of each loop were manipulated every 30 minutes to compensate the different optical efficiency of the loops. The results show that by manipulating the input valves to distribute the flow properly, energy gains can be expected. The algorithm computed the input valve opening in such a way that the more efficient loops received more flow and viceversa.

In this chapter a nonlinear model-based optimization control algorithm is presented to make the solar field as homogeneous as possible from the thermal point of view. A model of a 50 MW solar trough plant is used to test the algorithm. The plant is made up of 90 loops. The aperture of the input valves is computed every 5 minutes: the more efficient loops will receive a

higher flow and viceversa. The algorithm is compared to the case when the input valves are not manipulated. Better thermal distribution is obtained and thermal energy losses due to defocusing collectors are significantly reduced.

Another important issue to be addressed when operating large scale solar trough plants is the defocusing of collectors when the plant is working under power limitation requirements coming from the Transmission System Operator (TSO). In this case, the heat transfer fluid (HTF) flow is limited by the maximum power production and the temperature has to be controlled by defocusing the collectors to avoid overheating problems which degrade the HTF. This chapter presents MPC control techniques dealing with the problem of power limitations and controlling temperature by defocusing collectors. Several results of the controllers in different scenarios are given. Further information about operational problems under power limitations and temperature regulation by defocusing collectors can be found in [20]. Recently, an adaptative model predictive control scheme was presented in [21]. This adaptative scheme outperforms the one proposed in [20].

The chapter is organized as follows: section 2 describes the mathematical model of the 50 MW solar parabolic trough plant used in this chapter. Section 3 presents the flow-rate model predictive control scheme used to regulate the average temperature of the whole solar field by manipulating the HTF flow. Section 4 describes the problem of operating the plant under power limitation restrictions and presents MPC control techniques to address this situation. Finally, section 5 presents the problem of achieving an adequate thermal balance in large scale solar plants and develops a nonlinear model-based optimization algorithm to deal with this problem.

2. PARABOLIC TROUGH FIELD MODEL

Research works have used the ACUREX solar plant model for design and testing. The ACUREX field, located at the Plataforma Solar de Almería,

consists of 480 parabolic trough collectors. The collectors are arranged in 10 loops, each one composed of two rows of 12 modules. The total length of each loop is 172 m, which comprises active parts (142m) and passive parts, i.e., joints and other parts not reached by concentrated radiation (30 m).

Although ACUREX has been an excellent platform for research and experimentation which has promoted the development of solar technology, at present it is far from resembling a commercial plant, mainly due to its small size.

However, to design, simulate and present results here, it seems reasonable to use a plant model of approximately the dimensions and electrical production as in existing commercial plants. The chosen plant model is a 50 MW of electrical production without TES [22-24]. Plants that have thermal storage may, for a time, deal with power limitations by diverting part of the flow-rate to the TES. Plants that do not have thermal storage cannot divert flow-rate at any time.

Fairly widespread examples of commercial plants are those with a production of 50 MW without thermal storage such as [23, 25, 26]. In this chapter, we will describe a simulation model based on a 50 MW plant without TES. This model is later used for simulation and design of control strategies for defocusing, electric power and for thermal balance of the solar field.

A distributed parameter model is used to simulate the 50 MW solar trough field while a concentrated parameter model is used to design the Feed Forward series controller for disturbance rejection, [27, 28].

2.1. Parabolic Trough Field

The solar field of a 50 MW plant is, unlike the ACUREX field, extensive. As previously mentioned, the total length of each loop in ACUREX, is 172 m, whereas in a 50 MW commercial plant the length is around 600 m with 4 collectors for each loop [23, 25, 26]. The number of

loops is another important factor. In commercial plants (50 MW), there are around 90 loops [22-24, 26, 29, 30].

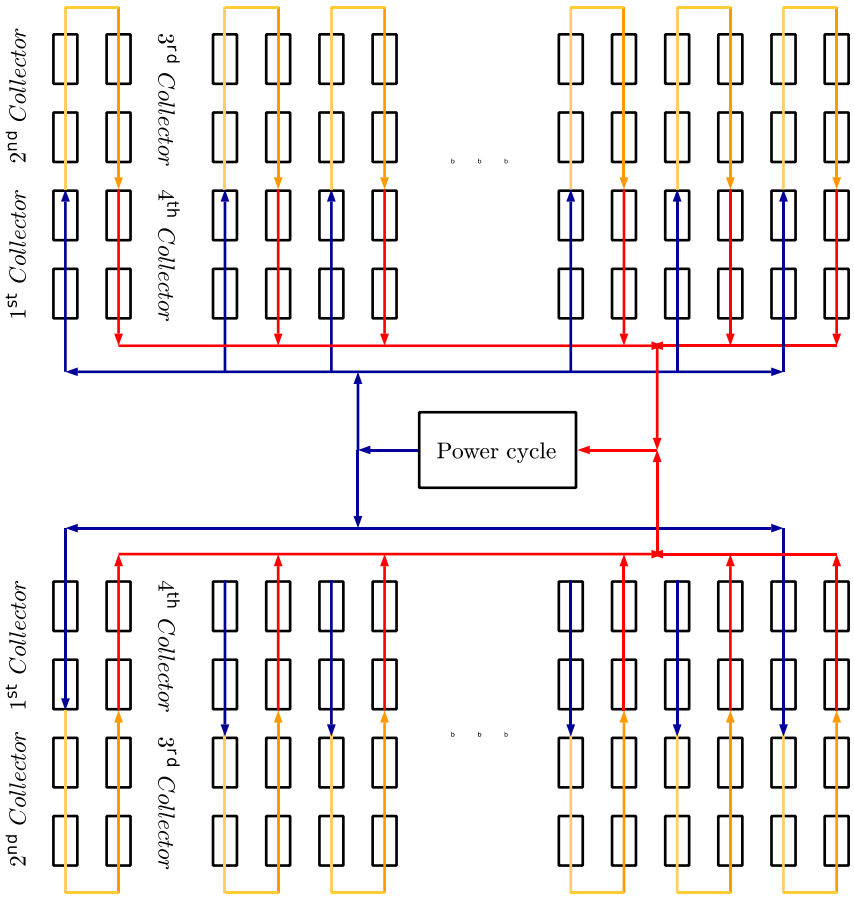

Figure 1. Parabolic trough plant general schematic.

For efficiency reasons, the orientation of the field of a commercial solar plant, is north-south, unlike ACUREX, which is east-west. The plant model used in this chapter for simulation and control design purposes consists of 90 600 meter loops where each collector is 150 m long. In Figure 1 a schematic parabolic trough plant is shown.

2.2. Collectors, Reciever Tube and Heat Transfer Fluid

For the 50 MW plant simulation model, the collector EuroTrough ET150 [31-33] is selected. In order to simulate the field, it is necessary to describe the collector in terms of parameters. In Table 1 the main parameters of the EuroTrough ET150 collector are shown [33-36]. Figure 2 shows a general schematic of a parabolic collector.

The receiver tube used in the model is the Schott PTR70 as it is one of the most commonly used in commercial plants [24, 25, 32]. The reader should refer to [37] for a complete description of Schott PTR70.

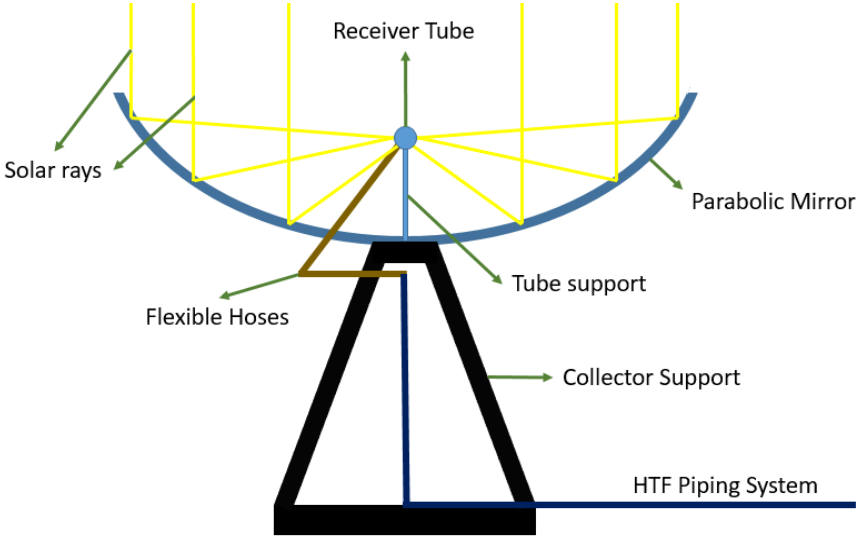

Figure 2. Parabolic collector general structure.

Table 1. EuroTrough ET150 parameters

Description	Value	Unit
Focal length	1.71	m
Aperture width	5.77	m
Aperture area	817.5	m^2

Number of Modules per Drive	12	Unitless
Length per Solar Collector Assembly (SCA)	148.5	m
SCAs per loop	4	Unitless
Heat Collection Element (HCE) Type	Evacuated tube	Unitless

The Heat Transfer Fluid (HTF) is used to generate the necessary steam for the steam power cycle. Therminol VP1 and DOWTHERM HTFs are the most used fluids in commercial solar plants. In this paper, Therminol VP1 is used. It is a synthetic thermal oil with a Diphenyl oxide/Diphenyl composition. This HTF can operate at temperatures between 12 °C and 400 °C, [38]. Above 400 °C the fluid degrades. Fluid density (ρ_f) and specific heat capacity (C_f) are temperature dependent and can be obtained by equations (1) and (2). The reader should refer to the manufacturer, [38], for more parameter approximations.

$$\rho_f = -0.90797 \cdot T + 0.00078116 \cdot T^2 - 2.367 \cdot 10^{-6} \cdot T^3 + 1083.25 \quad (1)$$

$$C_f = 4.5904 \cdot 10^{-8} \cdot T^4 - 3.1536 \cdot 10^{-5} \cdot T^3 + 0.006498 \cdot T^2 + 2.3458 \cdot T + 1500.8 \quad (2)$$

Power generation is proportional to the oil flow-rate and the HTF temperature drop at the steam generator. This temperature drop is approximately 90-100 °C in current plants with an outlet temperature of around 393 °C and field inlet temperature of 293 °C at nominal operation. An efficiency of the Rankine cycle of 0.381, [25, 32], is used. Parasitic effects, typically 0.9, which reduce generated power [33] and other losses or self-consumption are included as another efficiency. This efficiency has been assumed to be in the range of 0.9-1.

$$Q = \frac{P \cdot 10^6}{\Delta T \cdot C_f \cdot \eta_{rank} \cdot \eta_{par} \cdot \eta_{ext}} \quad (3)$$

Under these parameter assumptions and under nominal operation (inlet temperature closed to 293 °C, outlet temperature closed to 393 °C) the HTF flow-rate needed to produce 50 MW is in the range of 3025-3350 m^3/h,

approximately, using equation (3), [20], for a temperature drop of 95 °C in the generation cycle. The power cycle dynamic behavior varies according to the operating point of the flow-rate as shown in [39, 40]. For the simulations shown in this chapter, the generated power is computed using equation (3) and then filtered. The power generation dynamics have been approximated by first order linear models with time constants for the filters of 170, 260 and 400 seconds when the flow-rates are 2565, 1710 and 855 m^3/h at nominal temperature.

2.3. Distributed Parameter Model

The dynamics of the distributed solar collector field are described by the following system of partial differential equations (PDE) describing the energy balance [27, 28]:

$$\rho_m C_m A_m \frac{\partial T_m}{\partial t} = IK_{opt} n_o G - H_l G(T_m - T_a) - LH_t(T_m - T_f) \quad (4)$$

$$\rho_f C_f A_f \frac{\partial T_f}{\partial t} + \rho_f C_f Q \frac{\partial T_f}{\partial x} = LH_t(T_m - T_f) \quad (5)$$

where the subindex m refers to the metal and f refers to the fluid. The geometric efficiency depends on hourly angle, solar hour, declination, day of the year, local latitude and collector dimensions. Density ρ, specific heat C and coefficient H_t depends on fluid temperature. Thermal losses to the ambient depend on the difference between metal temperature and the ambient temperature in a fourth order polynomial approximation as shown in [41, 42]. Based on the thermal losses, coefficient H_l can be expressed as a third order polynomial, $H_l = a_0 + a_1(T_m - T_a)^3$.

The coefficient of heat transmission depends on temperature and oil flow [28]. H_t can be calculated with the equations (6-10), [38], for a turbulent flow-rate Q (m^3/s) inside a pipeline.

$$Re = Q \cdot D/(\nu \cdot A) \quad (6)$$

$$Pr = C_f \cdot \mu/k \tag{7}$$

$$phi = 1.023 \tag{8}$$

$$Nu = 0.025 \cdot (Re^{0.79}) \cdot (Pr^{0.42}) \cdot phi \tag{9}$$

$$H_t = Nu \cdot k/D \tag{10}$$

The model is discretized in the longitudinal dimension of the tube so the dynamics of each loop can be simulated as a chain of sub-models. A segment length of 1.98 meter has been chosen for the implementation of the simulation model (300 segments per loop). For the ACUREX plant, the chosen number of segments is typically 172 with a 1 meter length segment. This amount of segments provides good performance for the simulation of the field by using the distributed parameters model. However, the ACUREX loop length is 172 meters while in this case a 600 meter loop length is considered for the 50 MW plant simulation. A simulation with 300 approximately 2 meters long segment also provides good simulation performance and reduces the computation time. The number of segments can always be increased but with a higher computational cost. Reducing the number of segments too much will entail a loss in the nonlinear dynamic resolution of the field simulation.

2.4. Lumped Parameter Model

The Lumped parameter model (LPM) provides a general description of the whole field. This model describes the variation in the internal energy of the fluid by equation 11. This model will be used to implement the the series Feed-Forward control and to estimate the collector global efficiency.

$$C_{loop}\frac{dT_{out}}{dt} = K_{opt}n_oSI - qP_{cp}(T_{out} - T_{in}) - H_lS(T_{mean} - T_a) \quad (11)$$

where P_{cp} can be approximated by $1.868 \cdot 10^6$ J/m^{3}C, C_{loop} is approximated by $3.287 \cdot 10^6$ J/°C and S is equal to 3427 m^2 [20]. This model will be used to implement a series Feed-Forward controller.

3. FLOW-RATE MODEL PREDICTIVE CONTROL SCHEME

This section describes the control scheme used to perform outlet temperature tracking. A GS-GPC is used for the flow-rate control scheme and a series FF is used for disturbance rejection. The series FF has proved to be very effective at rejecting measurable disturbances affecting the solar field [28].

3.1. Generalized Predictive Control

The GPC algorithm is based on the following single-input single-output model [43]:

$$A(z^{-1})y_k = z^{-d}B(z^{-1})u_{k-1} + \frac{C(z^{-1})}{\Delta}e_k \quad (12)$$

where u_k and y_k are the control and output sequences of the plant, e_k is a zero mean white noise term and Δ is the integrator operator. A, B and C are polynomials in the backward shift operator z^{-1}:

$$A(z^{-1}) = 1 + a_1z^{-1} + \ldots + a_{na}z^{-na}$$
$$B(z^{-1}) = b_0 + b_1z^{-1} + \ldots + b_{nb}z^{-nb}$$
$$C(z^{-1}) = 1 + c_1z^{-1} + \ldots + c_{nc}z^{-nc}$$

where d is the dead time of the system and Δ is the operator $1 - z^{-1}$. This model is known as a Controller Auto-Regressive Integrated Moving-Average (CARIMA) model.

Consider a multistage cost function of the form:

$$J(N_1, N_2, N_u) = \sum_{j=N_1}^{N_2} \delta(j)[\hat{y}(k+j|k) - w(k+j)]^2 + \sum_{j=1}^{N_u} \lambda(j)[\Delta u(k+j-1)]^2 \quad (13)$$

where $\hat{y}(k+j|k)$ is an optimum j step ahead prediction of the system output, N_1 and N_2 are the minimum and maximum costing horizons, N_u is the control horizon, $\delta(j)$ and $\lambda(j)$ are weighting sequences and $w(k+j)$ is the future reference trajectory. The aim of GPC is to minimise $J(N_1, N_2, N_u)$ in order to compute a future sequence of control actions $u(k), u(k+1), \ldots$ that drives the future plant output $y(k+j)$ close towards $w(k+j)$.

Hence given a CARIMA plant model and suitable cost function, the minimum of the cost function can be obtained by setting the gradient of J equal to zero and solving the control sequence $\mathbf{\Delta}$u by the following equation [43]:

$$\mathbf{\Delta}\mathrm{u} = (GG^T + \lambda I)^{-1} G^T (w - f) \quad (14)$$

where matrix G contains the step response coefficients of the forced response model [12], I is the eye matrix, f is the free response of the plant, w is the future reference trajectory vector and λ is the control weighting vector [43].

3.2. Gain Scheduling

The design of the GS-GPC is described in [28, 44]. The GS-GPC controller has demonstrated to have very good behaviour not only in respect to set-point tracking but also in disturbance rejection capabilities [28]. Depending on the point at which the system operates, the GS-GPC feedback gain is adjusted in order to compensate variation in the plant response under

different working conditions. In a solar trough plant, the dynamic is mainly dictated by the oil flow. Four oil flow levels covering the operation range of the plant are used (1494, 1908, 2322 and 2736 m^3/h). Since the linear models correspond to the FF plus the plant model, the input is the temperature reference from GS-GPC (input to FF) and the output is the outlet oil temperature (output of the plant) ($^\circ C$).

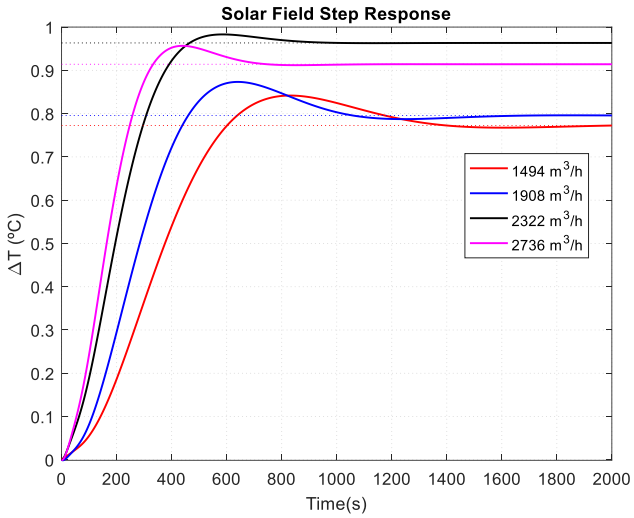

Figure 3. Solar field step response of linear models. Output increments when unitary steps are applied to the input.

A suitable identification of the model parameters at four different set-points for the oil flow (1494, 1908, 2322 and 2736 m^3/h) will be used. Step responses are shown in Figure 3. The GS-GPC has been designed assuming that the parameters of all loops are the same. It is also assumed that the field is balanced, therefore the flow going into each of the loops is the same and therefore, global dynamic model based on one loop is used to design the GS-GPC.

3.3. Series Feed-Forward Control

The use of a series Feed-Forward controller action has proved to be very effective at rejecting solar radiation disturbances when using linear controllers. Moreover, it contributes significantly to preserving the validity of the assumed linear description of the plant over all its operation range. The FF input signal is a temperature set-point from GS-GPC control, while the control output is the oil flow-rate, q_{ff},which is computed by the lumped parameter description [45]:

$$q_{ff} = \frac{K_{opt} n_o SI - H_l S(T_{mean} - T_a)}{P_{cp}(T_{ref} - T_{in})} \quad (15)$$

The control algorithm works as follows: The GS-GPC receives the temperature set-point for the solar field and the current mean temperature and computes a virtual reference temperature, T_{ref}, for the FF. The FF computes the oil flow taking into account the virtual reference and the measured disturbances to track the desired set-point. Since the GS-GPC + FF scheme is considering the global model as the model of one representative loop, the calculated flow-rate is for one loop, q_{ff}.

The GS-GPC + FF scheme is presented in Figure 4 where $Q_{ff} = q_{ff} \cdot NL$ and NL is the number of loops (all loops are assumed to receive the same amount of HTF, hydraulic balance) and Q is the solar field measured flow-rate. Figure 5 shows a simulation of the GS-GPC + FF control scheme showing that the controller correctly tracks the temperature set-point.

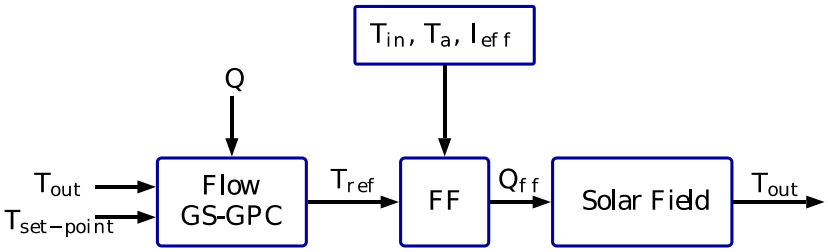

Figure 4. GS-GPC + FeedForward control scheme.

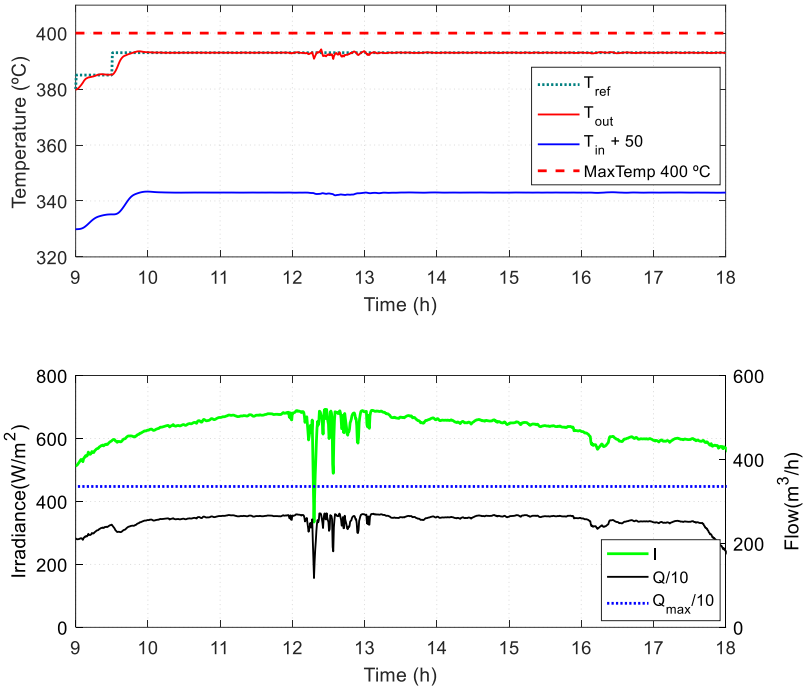

Figure 5. GS-GPC + FF tracking results (medium-high solar irradiance).

4. Collector Defocus and Power Limitation Model Predictive Control

This section describes the design of the controller for defocusing the collectors and for power control. Defocus control is important in order to keep the oil temperature within the limits provided by the manufacturer and to avoid its degradation. There are occasions when the plant may receive power limitation commands from the Transmission System Operator (TSO), generally, when the electrical grid is saturated. The operation of controlling the power at a certain point is usually a complicated task for the operators due to the very nature of the constraint, the disturbances and the plant dynamic behavior. In this section, MPC controllers are presented for defocus and power control. First, the defocus control for the fourth collector is presented. Subsequently, the problem of power limitations in commercial

plants is explained. A controller that is activated in cases of power limitation is presented. Another controller for the defocusing of the third collector is also introduced, since in power limitations fourth collector defocus control may not be enough to maintain the plant within the safety limits. Finally, the results of the controllers in different scenarios are presented.

4.1. Fourth Collector Defocus GS-GPC

As presented in Figure 5, the GS-GPC in series with an FF correctly tracks the field outlet temperature set-point because this simulation corresponds to a medium irradiance day. Flow-rate in this simulation is close to the maximum. On a high irradiance day, flow-rate control is not enough to control the outlet temperature and, thus, the temperature will rise rapidly. Figure 6 shows this scenario where the flow-rate is at its maximum and the outlet temperature rises progressively until it exceeds the maximum temperature.

Generally, parabolic trough plants have safety mechanisms to prevent the outlet temperature of a loop exceeding the allowed maximum. This security procedure is carried out by defocusing the collectors, causing the loop to cool down due to the decrease in the amount of effective radiation received by the tube. The defocusing of the fourth collector is, generally, applied simply to prevent the oil temperature from exceeding a maximum temperature of 400 °C. This control action is carried out by modifying the angle of the collector. Moreover, fourth collector defocus of one loop is independent of the defocus actions of other loops since each loop is different and their parameters may vary amongst themselves so that not all loops will be at the same temperature.

Given that this strategy is a security procedure, it is generally applied in a staggered manner as total or partial defocusing. Working in such way, it is highly inefficient due to the thermal jumps caused by the application of partial or full defocusing. Since it is usually carried out by the use of thresholds, this defocusing mechanism is reactive and may cause oscillations in the outlet temperature of the loops.

Although, at first glance, this may not seem an important problem in the control of solar plants given the large dimensions of commercial plants (90 to 800 loops). However, the oscillations caused by sudden actions in defocusing the collectors, can lead to energy losses, dynamics couplings and deterioration of the actuators.

Instead of working with thresholds, it is possible to apply MPC techniques for tracking the loop outlet temperature and avoiding abrupt defocus control actions. In this chapter, a possible solution to the defocusing problem by designing an Event based GS-GPC is proposed for fourth collector defocus control. As mentioned, the defocusing of the loops is independent and therefore an EGS-GPC is needed per loop. This controller is designed in a similar way to the flow-rate GS-GPC. Approximate models must be obtained at different points of operation to design the gain scheduling which is then integrated with a GPC controller, although in this case it does not include a Feed-Forward controller.

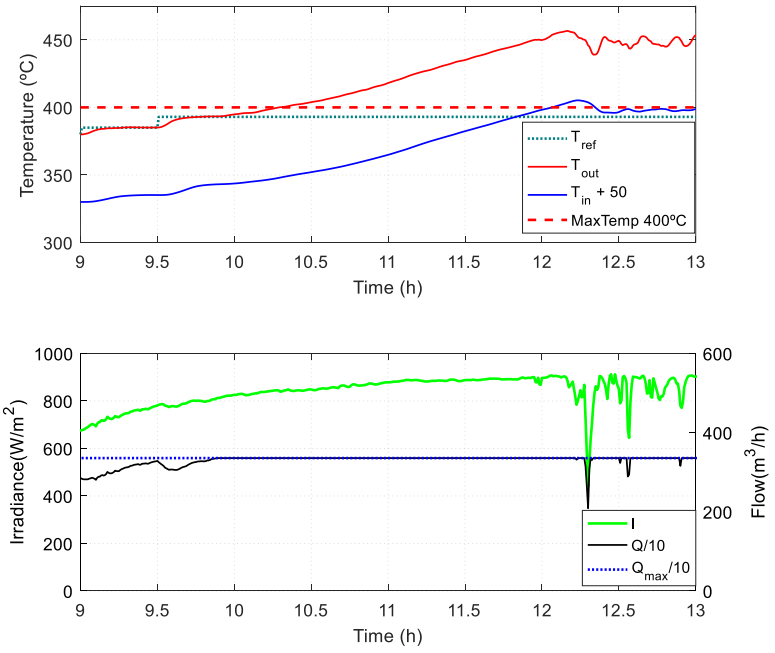

Figure 6. GS-GPC + FF. Flow-Rate at maximum due to high irradiance leading to temperature limit violation.

In order to design a defocus control, a function that relates the defocus angle and collector efficiency is needed. The approximation of this function to design the GS-GPC is presented in Figure 7, [1]. Since the function is non-linear, the gain-scheduling will be designed at 9 different points of defocus angle (0.5, 1, 1.5, 2, 2.5, 3, 3.5, 4 and 4.5 degrees). From a certain defocus angle, efficiency begins to decrease rapidly, since rays no longer reach the tube. Moreover, the plant responds differently depending on the flow-rate, so defocus linear models will not be the same for all flow-rates. To improve the performance of collector defocus GS-GPC, 9 linear models are obtained for each of the flow-rate points where Flow GS-GPC has been designed (1494, 1908, 2322 and 2736 m^3/h). The linear models obtained are presented in Figures 8 and 9.

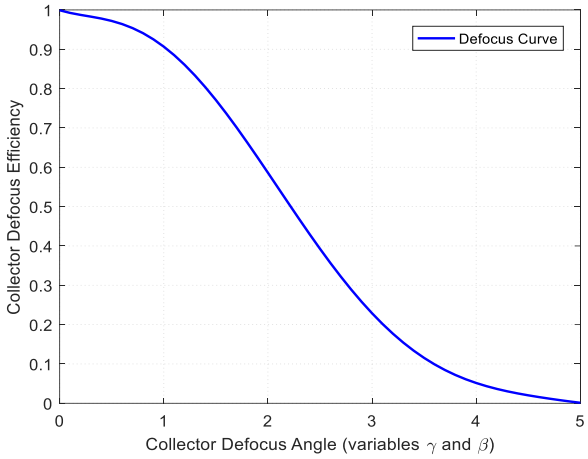

Figure 7. Efficiency - Defocus angle curve.

Regarding the temperature set-point, it is easier to apply one of 393 °C to each loop given that it is the nominal working temperature. However, the loops may vary in reflectivity, tube efficiency and form factor, amongst others things, and some loops may be colder than others. In the hotter loops, defocus would be activated for a temperature reference of 393 °C and the other loops would be at a slightly lower temperature. At certain times this

could cause a conflict with flow-rate control. To avoid this, an event based heuristic is applied to send different temperature set-points to the GS-GPC. This heuristic is to detect an event, based on flow-rate and outlet temperature, to apply the appropriate set-point:

Algorithm 1: Saturation event detection (C4 set-point)

Input: $Q(k)$, $T_{out}(k)$

Output: T_{ref-C4}

1: **if** $Q(k) > Q_{high}$ & $T_{out}(k) > T_{high}$ **then**

2: $T_{ref-C4} = T_{ref-sat}$

3: **else if** $Q(k) < Q_{low}$ or $T_{out}(k) < T_{low}$ **then**

4: $T_{ref-C4} = T_{ref-nosat}$

5: **end**

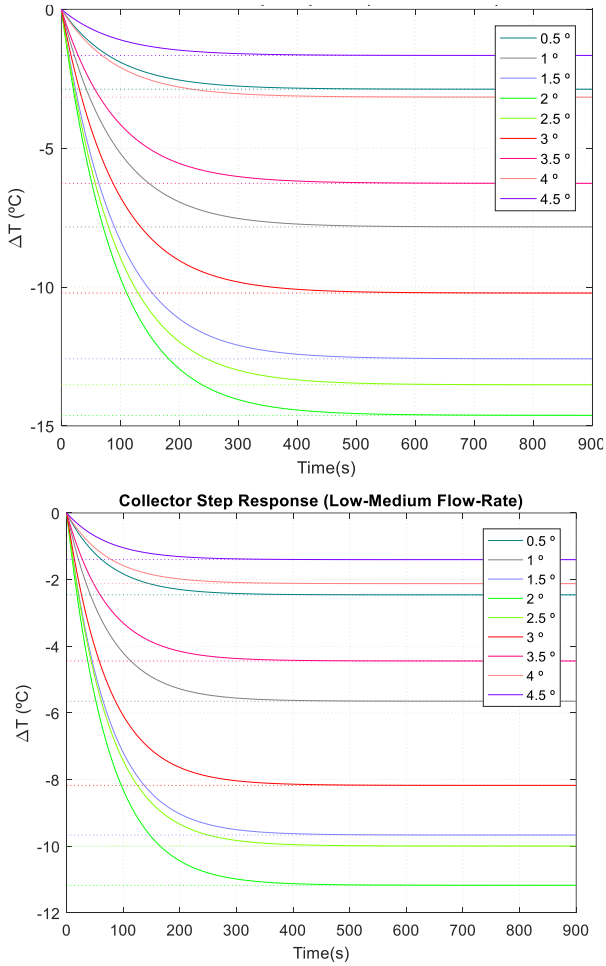

Figure 8. Collector step response of linear modelsfor low and low-medium flow-rates.

These are simple rules that allow the controller to autonomously apply a different temperature set-point according to the state of the plant. If the plant is near the maximum flow ($Q(k) > Q_{high}$) and at a field outlet temperature (weighted average of the loops outlet temperatures) greater than T_{high}, then the applied temperature set-point will be the nominal temperature (393 °C). This is done because in this situation the flow cannot control the outlet temperature which at this stage can only be controlled by defocusing. When the flow is relatively far from the maximum available or

the field outlet temperature is below the limit, the set-point may increased. This is to take advantage of the higher temperature provided by the hottest loops since not all loops will be in the same condition of efficiency. The hottest loops compensates for the coldest in order to obtain the desired field output temperature with greater efficiency.

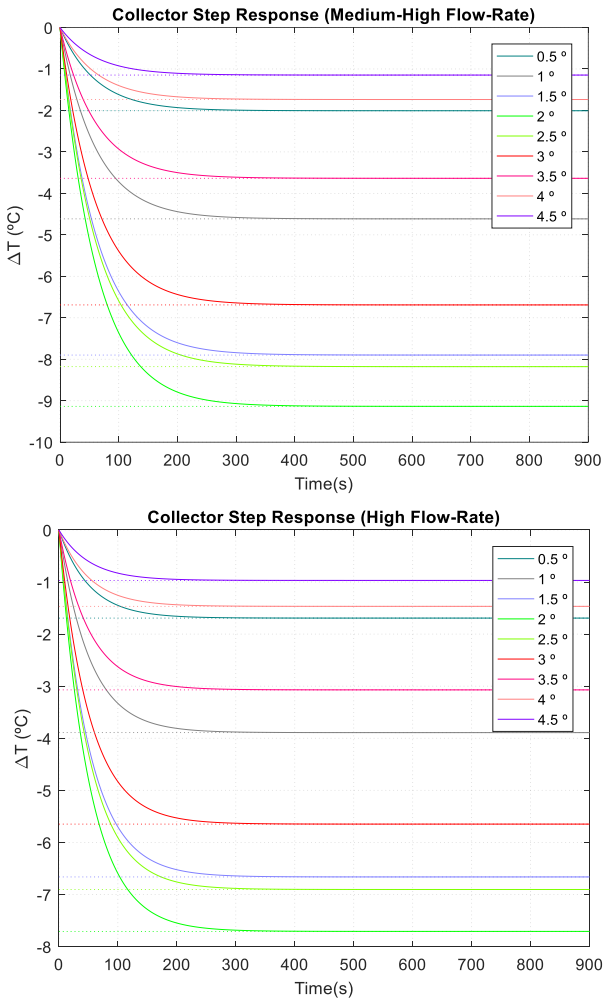

Figure 9. Collector step response of linear models for medium-high and high flow-rates.

In this case, the chosen values for previous set-points are: $Q_{high} = 3150$ m^3/h, $Q_{low} = 3060$ m^3/h, $T_{high} = 395$ °C, $T_{low} = 391$ °C, $T_{ref-nosat} = 396$ °C and $T_{ref-sat} = 393$ °C. The control scheme including flow-rate and defocus controllers is presented in Figure 10.

In Figures 11 and 12, results of the simulation of the flow GS-GPS adding the event based defocus GS-GPC is shown. In this simulation, where irradiance is high, it can be seen how by defocusing the fourth collector it is possible to maintain the temperature below the maximum limit.

In general, in normal situations, defocusing the fourth collector is enough to avoid outlet oil temperature from reaching the limit indicated by the manufacturer. However, there may be other situations in which something else is needed to avoid overheating and deterioration of the oil and collectors. This situation is explained in the next section and it is when the plant is under power limitation commands.

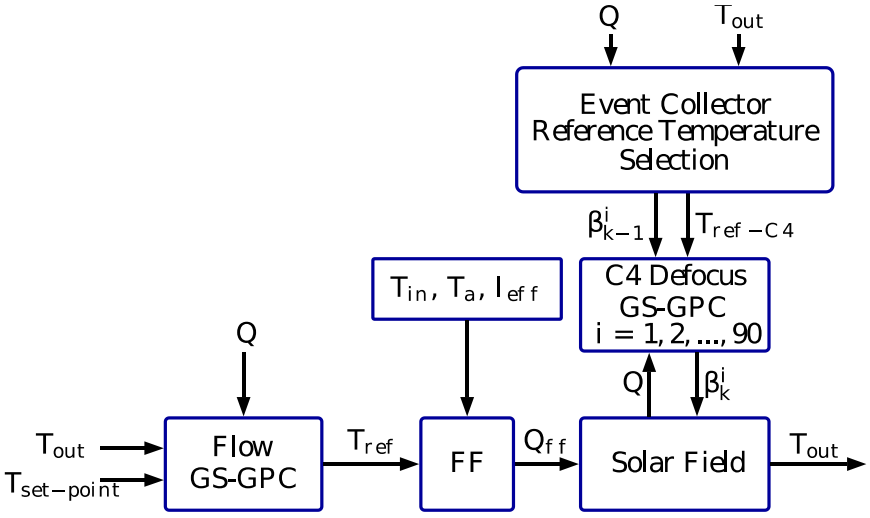

Figure 10. Flow GS-GPC + FF + C4 EGS-GPC control scheme.

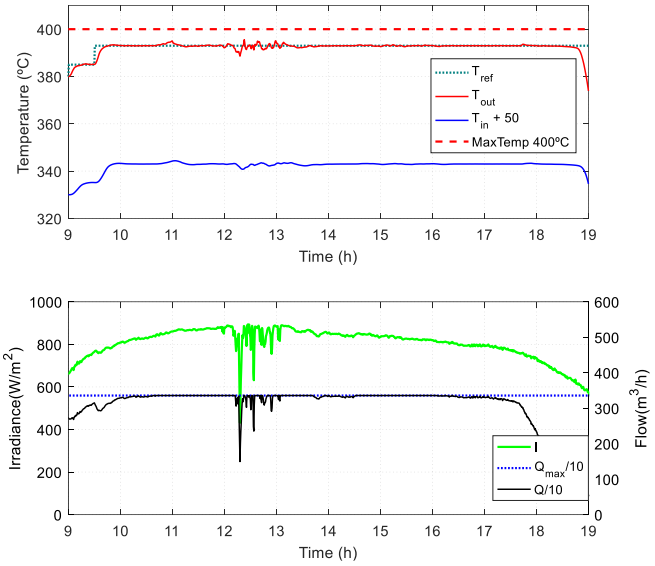

Figure 11. Flow GS-GPC + FF + C4 EGS-GPC loop temperature tracking results. Top plot: field temperature. Bottom plot: Irradiance and flow-rate.

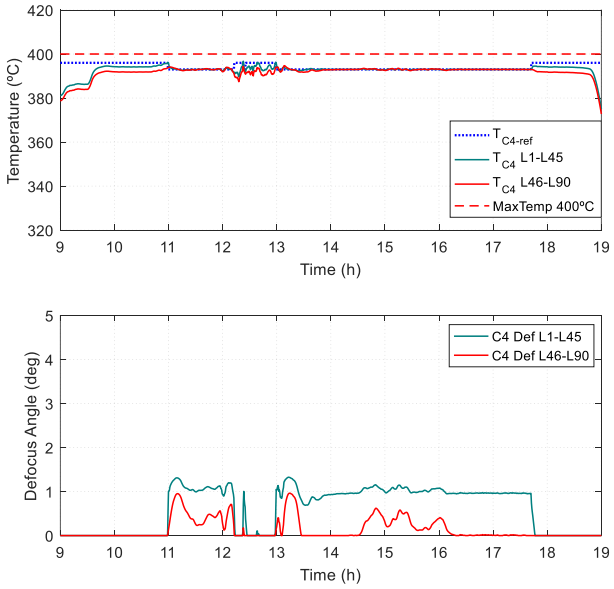

Figure 12. Flow GS-GPC + FF + C4 EGS-GPC loop temperature tracking results. Top plot: loop temperature. Bottom plot: Fourth Collector defocus angle control actions.

4.2. Commercial Plants under Power Limitations

One of the most important factors in commercial plants is the optimization of plant operation. The aim of commercial plants is to produce the maximum amount of electricity..

However, there are situations in which a plant has to move into an operation mode in which optimization of the power produced does not make sense. A commercial solar plant may receive commands of power limitation from the TSO, typically, when the electrical grid is saturated. In these cases, the plant is forced to decrease its electric production and maintain the power set-point determined by the TSO. Maximum power production no longer makes sense. In these situations the objective is double: fulfilling the TSO power set-point and temperature tracking. The nominal operating point of a commercial plant is generally around 393 °C [24, 26]. The plant has a time period to reduce the electric power to the set-point determined by the TSO. If the plant does not comply with the determined set-point it faces economic sanctions. To decrease power, it is necessary to decrease the oil flow-rate that reaches the heat exchanger where the steam phase begins.

Plants with Thermal Energy Storage (TES) are able to deal with this situation, at least for a while, by diverting part of the flow-rate to the TES, until these are saturated. Plants without TES cannot cope so easily. This chapter, focuses on plants that do not have TES such as [22-24, 26].

Decreasing the flow-rate increases the outlet temperature. However, if the flow-rate is used to control the power, the defocus mechanism is necessary to control the field outlet temperature at the nominal operating point. In the following sections, it is shown that fourth collector defocusing control may not be enough to maintain the outlet temperature at the desired temperature and extra control is needed. Before presenting a solution to this problem, the design of a GS-GPC for the control of power, which is activated only in cases of power limitation, is presented. It will be shown that defocusing the fourth collector is not enough to maintain the plant at safe temperature levels in cases of imposed power limitations.

4.3. Power Generation Event Based GS-GPC

To design power GS-GPC control, first order systems are approximated at 3 flow-rate working points 855, 1710 and 2565 m^3/h (167.06, 334.1 and 501.16 kg/s) at nominal temperature 393 °C. Figure 13 shows the output increment when a unitary step is applied to the input at different operating points. The design of the GS-GPC is done in the same way as in the cases of the flow-rate and fourth collector defocus controllers.

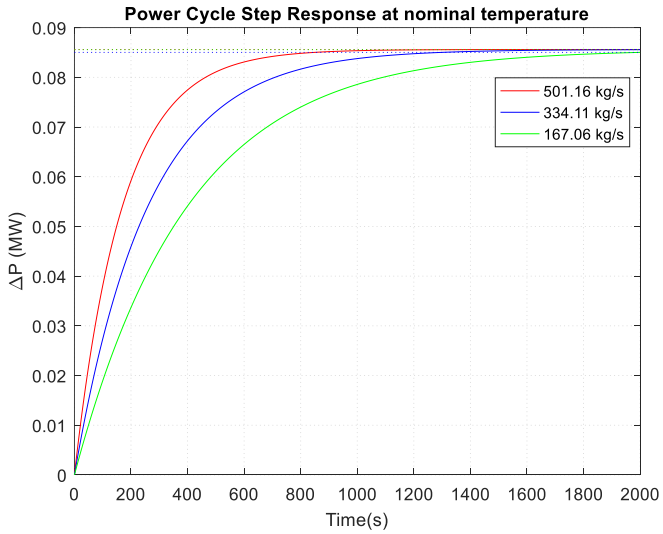

Figure 13. Power cycle step response of linear models. Output increments when unitary steps are applied to the input.

Upon receiving a TSO power limitation, the plant has time to adjust to the set electric power limit. In general, this is a complex operation for an operator, given that the flow-rate must decrease in order to reach the power set-point in a given time. Since the power cycle can be modeled as linear systems, an Event based GS-GPC is proposed to control the electric power generated by the plant. In this case, the event is none other than power limitation determined by the TSO. The use of MPC is a great advantage, since a power reference ramp for the time available can be used to obtain better response due to the sliding horizon. Generally, in many processes the

set-point is fixed and future set-points are unknown. However, in this case, it is possible to take advantage of the use of the MPC sliding horizon since it is possible to create time ramp power set-points (future set-points). This will improve and make smoother power set-point tracking than with a simple power step.

Power limitations received by the TSO will be implemented as boolean variables, TSO_L and PW_{TSO}. These variables will be set to true when the TSO limitation is received (down-ramp starts). TSO_L will be set to false when the TSO limit has been removed and PW_{TSO} will be set to false in two situations: (1) when the up-ramp is finished (TSO limit has been removed and the plant has reached 50 MW once again); (2) when during the up-ramp, the field outlet temperature is less than 391 °C, which means the plant cannot reach 50 MW at nominal outlet temperature, see Figure 14.

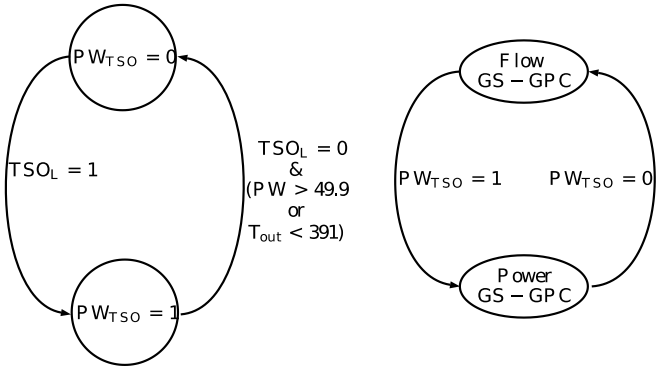

Figure 14. Power Limitation Event block state graph.

Due to the power limitation, the rules for applying the set-point temperature for defocus control must be modified. Since the flow is going to be reduced in order to reduce the power, the loops will begin to warm up as mentioned. In situations of power limitation the safest set-point for the defocus control should be applied. In this case a set-point of 393 °C is applied. The complete system of rules for applying the temperature set-point is as follows:

Algorithm 2: Power limitation/saturation event detection (C4 set-point)

Input: $PW_{TSO}(k)$, $Q(k)$, $T_{out}(k)$

Output: T_{ref-C4}
1: **if** $PW_{TSO}(k)$ or $(Q(k) > Q_{high}$ & $T_{out}(k) > T_{high})$ **then**
2: $T_{ref-C4} = T_{ref-sat}$
3: **else if** $Q(k) < Q_{low}$ or $T_{out}(k) < T_{low}$ **then**
4: $T_{ref-C4} = T_{ref-nosat}$
5: **if** $PW_{TSO}(k-1)$ & $!PW_{TSO}(k)$ **then**
6: $T_{ref-C4} = T_{ref-nosat}$
7: **end**

In order to reduce the electric power generated, the oil flow-rate will be considerably reduced, though the temperature will not decrease since the operation of the plant must remain at a nominal temperature of 393 °C.

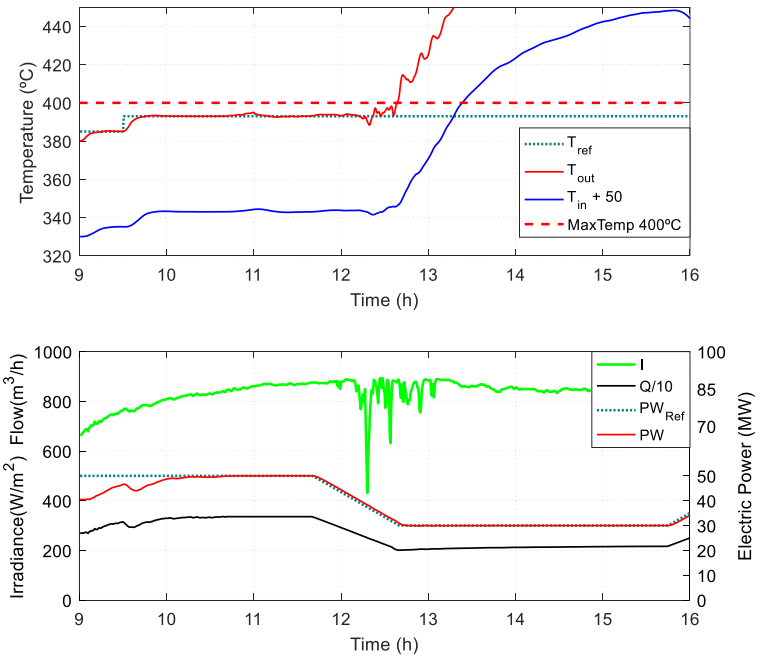

Figure 15. Flow GS-GPC + FF + Power EGS-GPC + C4 EGS-GPC outlet temperature limit violation. Top plot: field temperature. Bottom plot: Irradiance, flow-rate and electric power.

As previously mentioned, decreasing the flow-rate causes an increase in the outlet temperature of the loops that is controlled by the fourth collector defocus EGS-GPC. In normal situations, the defocus of the fourth collector

will have ample capacity to maintain the system at the point of operation without risk, as can be seen in Figures 11 and 12, where there is no power limitation. Depending on the power limitation command, the flow-rate will have to be decreased to a level at which the fourth defocus controller will not be able to keep the oil temperature below the temperature limit and the third collector needs to be defocused. Figures 15 and 16 illustrate this situation. This scenario shows the simulation results when a 30 MW power limitation is received by the TSO. The plant will have 60 minutes to reach the power set-point.

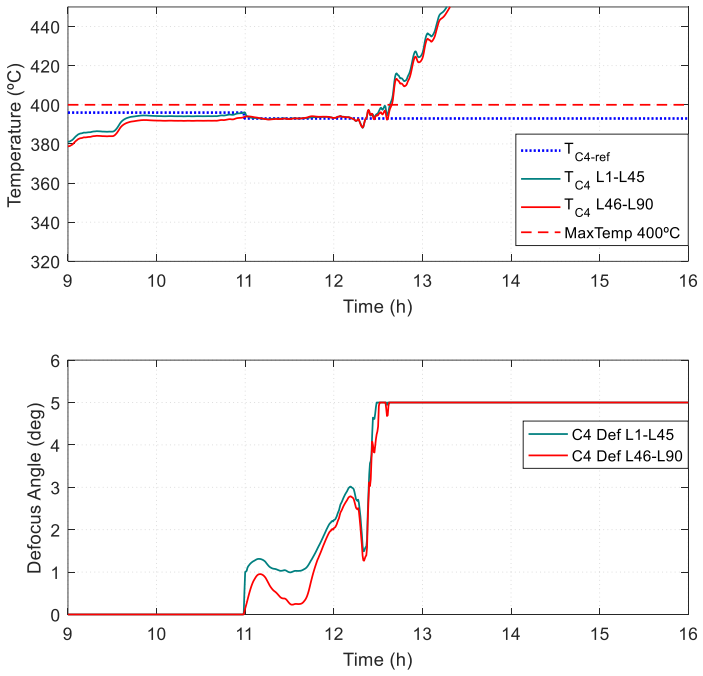

Figure 16. Flow GS-GPC + FF + Power EGS-GPC + C4 EGS-GPC outlet temperature limit violation. Fully defocused fourth collector. Top plot: loop temperature. Bottom plot: Fourth collector defocus angle.

The plant is generating approximately 50 MW when receiving the power set-point. In Figure 15, it can be observed how the temperature cannot be controlled at the desired temperature set-point due to the saturation of the fourth collector EGS-GPC control action, see Figure 16.

4.4. Third Collector Defocus GS-GPC

Defocusing of the third collector is necessary during a power limitation operation since the fourth collector controller will not be able to control the outlet temperature by itself. For control of the third collector of each loop, a GS-GPC event based is proposed, where in this case, the event is the limitation of generated electric power. The GS-GPC is designed in the same way as for the fourth collector. The linear models for gain scheduling the third collector are the same models previously calculated for the fourth collector, since they are collector models.

Since defocusing the third collector is not necessary ther than in power limitation, the event to be detected is the arrival of a power restriction. The temperature reference differs from the one used for the fourth collector. The simplest option would be to divide the desired thermal difference in the loop (100 °C) amongs the 4 collectors, which would result in a set-point of 375 °C for the third collector outlet temperature. However, the temperature set-point for the third collector has been chosen based on the control action of the fourth collector.

As previously mentioned, the defocusing curve is nonlinear. It can be seen how the curve has a steep slope around 2-3 degrees of defocus. Beyond 3 degrees, the efficiency approaches zero, which means very little control ability. The temperature set-point that the third collector must follow has been chosen around this defocusing angle. In this way, the third collector does not defocus until the GS-GPC of the fourth collector begins to lack control capacity. By simulation, it has been obtained that the approximate temperature value at the outlet of the third collector is 385 °C when the fourth collector is defocused around 3 degrees.

During the power reference up-ramp, the third collector is still active and, since the flow-rate is increased, in order to increase power, the temperature of the third collector will decrease causing the GS-GPC to decrease the control action until 0 degrees of defocus is reached. At the end of the up-ramp, the third collector will not be out of focus and only the fourth

EGS-GPC will be active. Similarly, when the up-ramp is terminated, the power EGS-GPC is deactivated and the flow-rate GS-GPC is activated once more in order to control the field outlet temperature at 393 °C. The full control scheme is presented in Figure 17.

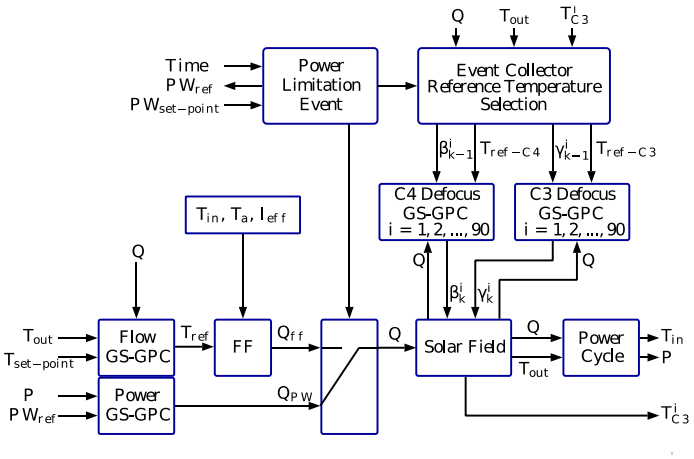

Figure 17. Flow GS-GPC + FF + C4/C3 EGS-GPC + Power EGS-GPC control scheme.

4.5. Simulation Results

In this section, results from simulations are presented. The simulations were carried out in scenarios with power limitations of one hour and half hour time constraints from the TSO. These scenarios have been simulated assuming that half the solar field has an overall efficiency of 0.7776 (45 loops) and the other half an efficiency of 0.7607 (45 loops). It has been done in this way since, although there is no problem in simulating and controlling a field with 90 loops, it is not possible to represent the control actions of 90 collectors in the same or in several graphs due to the space that this would take. A scenario in which 10 loops have different efficiencies has been simulated, to show the results of the defocus control actions of the third and fourth loop collectors.

First, it is shown that the third control may be unnecessary if the power set-point is not too low. In this scenario, a simulation of a 40 MW limitation

has been performed. Secondly, a scenario with a higher power limitation is simulated to show why the third collector defocus is necessary in case of power limitations.

Figures 18 and 19 show the results obtained from the proposed control scheme when receiving a power limitation of 40 MW with a one hour time constraint. At 11:40 a set-point of 40 MW is received from the TSO. At this point the plant is operating in flow-rate GS-GPC at 50 MW and 393 °C. Upon receiving the command, the plant begins to decrease the flow-rate to track the power reference indicated by the ramp that has been generated by the block “power cycle event”.

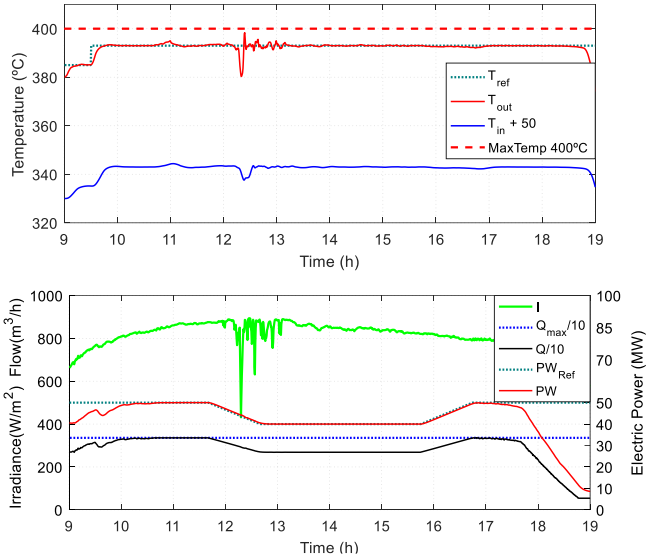

Figure 18. Flow GS-GPC + FF + C4 EGS-GPC + Power EGS-GPC, 40 MW TSO limitation at 11:40am and TSO limitation off at 15:45pm (60 min ramp). Top plot: field fluid temperatures. Bottom plot: Irradiance, flow-rate and electric power.

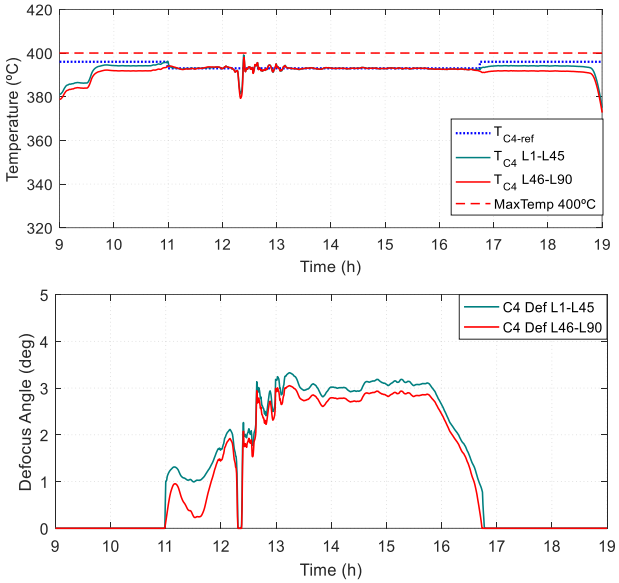

Figure 19. Flow GS-GPC + FF + C4 EGS-GPC + Power EGS-GPC, 40 MW TSO limitation at 11:40am and TSO limitation off at 15:45pm (60 min ramp). Top plot: loop fluid temperatures. Bottom plot: Fourth Collector defocus angle control actions.

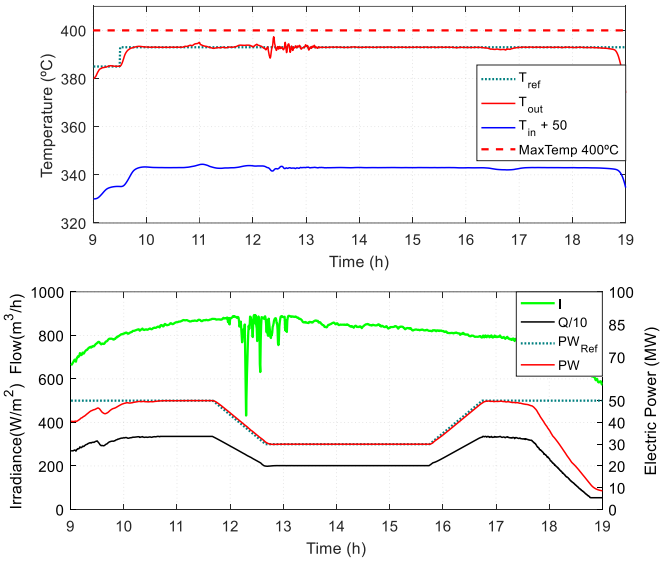

Figure 20. Flow GS-GPC + FF + C4/C3 EGS-GPC + Power EGS-GPC, 30 MW TSO limitation at 11:40am and TSO limitation off at 15:45pm (60 min ramp). Top plot: field fluid temperatures. Bottom plot: Irradiance, flow-rate and electric power.

As the flow rate decreases, the fourth collector defocus EGS-GPC is responsible for maintaining the loop outlet temperature at 393 °C, and thus the field outlet temperature too, since the plant is in power limitation. Figure 19 shows how the fourth collector EGS-GPC is able to correctly track the temperature reference.

Figures 20, 21 and 22 show the results of the same scenario when the third collector controller is added to the control strategy.

It is clear that third collector defocus helps to keep the outlet temperature of the field at the desired set-point. As previously commented, it starts to control when the outlet temperature of the third collector is close to 385 °C.

In Figure 21, it is possible to check that the fourth collector is at an angle control action in which it is still in control of the system.

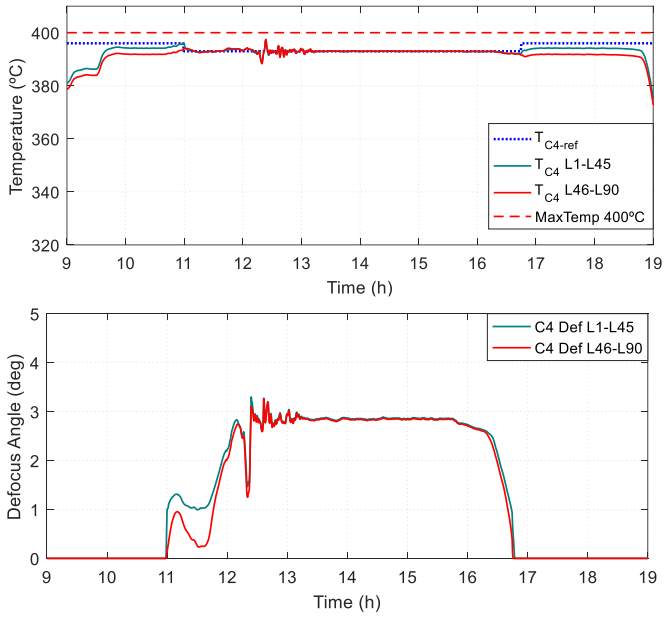

Figure 21. Flow GS-GPC + FF + C4/C3 EGS-GPC + Power EGS-GPC, 30 MW TSO limitation at 11:40am and TSO limitation off at 15:45pm (60 min ramp). Top plot: loop fluid temperatures. Bottom plot: Fourth collector defocus angle.

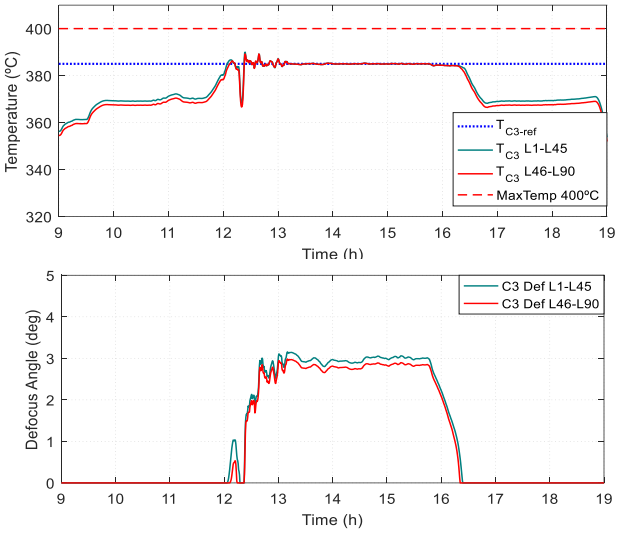

Figure 22. Flow GS-GPC + FF + C4/C3 EGS-GPC + Power EGS-GPC, 30 MW TSO limitation at 11:40am and TSO limitation off at 15:45pm (60 min ramp). Top plot: loop fluid temperatures. Bottom plot: Third collector defocus angle.

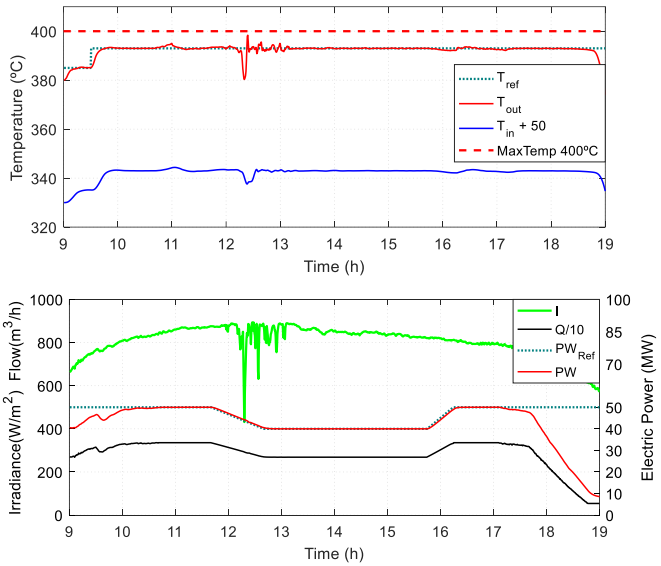

Figure 23. Flow GS-GPC + FF + C4/C3 EGS-GPC + Power EGS-GPC, 40 MW TSO limitation at 11:40am (60 min ramp) and TSO limitation off at 15:45pm (30 min ramp). Top plot: field fluid temperatures. Bottom plot: Irradiance, flow-rate and electric power.

Both controllers react against the radiation perturbation and continue defocusing until power limitation is off at 15:45 pm, see Figures 21 and 22. Power generation is increased when the limitation is removed and the third collector defocus GS-GPC drops to 0 degrees (efficiency = 1), see Figure 22.

In Figures 23, 24 and 25, a scenario with a 40 MW power limitation has been simulated with two different time periods. First, a time period of one hour to bring down power is received. The second time period is when the limitation is removed. The plant has half an hour to return to maximum possible production.

Figure 23 shows good performance of the controller tracking the power set-point in both ramps and the 40 MW TSO power limitation. Flow-rate is decreased during the down ramp and increased in the up ramp. During power limitation, the fourth collector EGS-GPC is the main controller acting over the system and keeping the outlet temperature at the desired set-point.

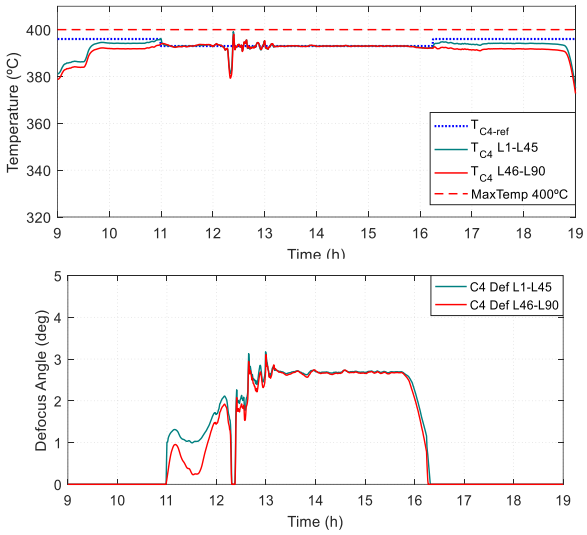

Figure 24. Flow GS-GPC + FF + C4/C3 EGS-GPC + Power EGS-GPC, 40 MW TSO limitation at 11:40am (60 min ramp) and TSO limitation off at 15:45pm (30 min ramp). Top plot: loop fluid temperatures. Bottom plot: Fourth collector defocus angle control actions.

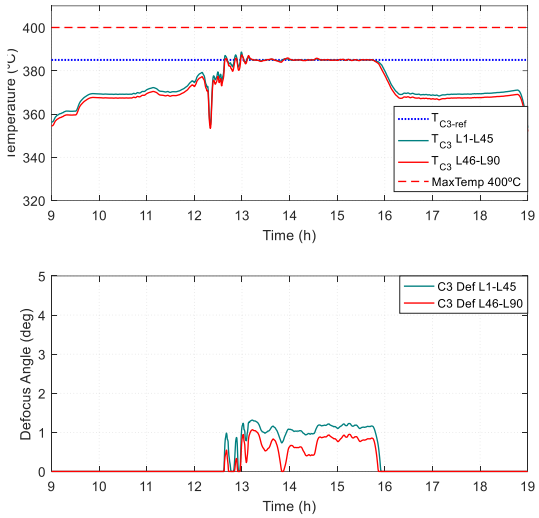

Figure 25. Flow GS-GPC + FF + C4/C3 EGS-GPC + Power EGS-GPC, 40 MW TSO limitation at 11:40am (60 min ramp) and TSO limitation off at 15:45pm (30 min ramp). Top plot: loop fluid temperatures. Bottom plot: Third collector defocus angle control actions.

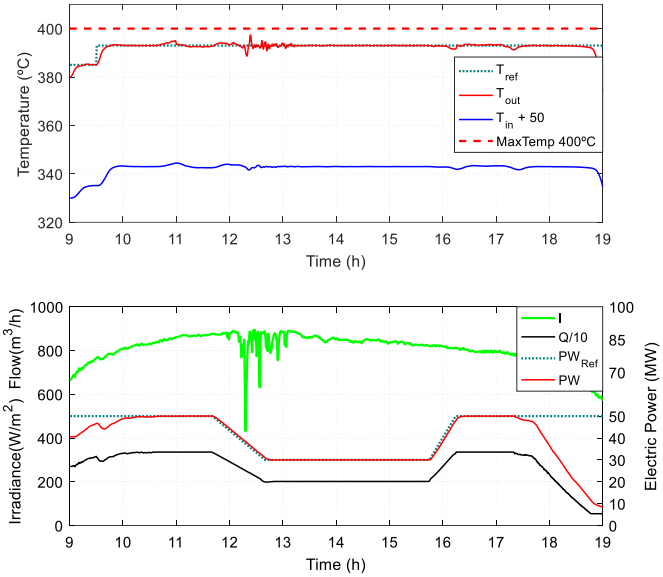

Figure 26. Flow GS-GPC + FF + C4/C3 EGS-GPC + Power EGS-GPC, 30 MW TSO limitation at 11:40am (60 min ramp) and TSO limitation off at 15:45pm (30 min ramp). Top plot: field fluid temperatures. Bottom plot: Irradiance, flow-rate and electric power.

Figure 25 shows that the third colletor GS-GPC is also active but with less control action in this case. Once again, it can be observed in Figures 24 and 25, that the set-point tracking of fourth and third collectors has good performance.

The last scenario shown in this section is a 30 MW power limitation, again with two time periods for the ramps and a set of different reflectivities for ten loops, see Table 2, to show the behaviour of the fourth and third controller applied to each loop. This scenario is shown in Figures 26, 27 and 28.

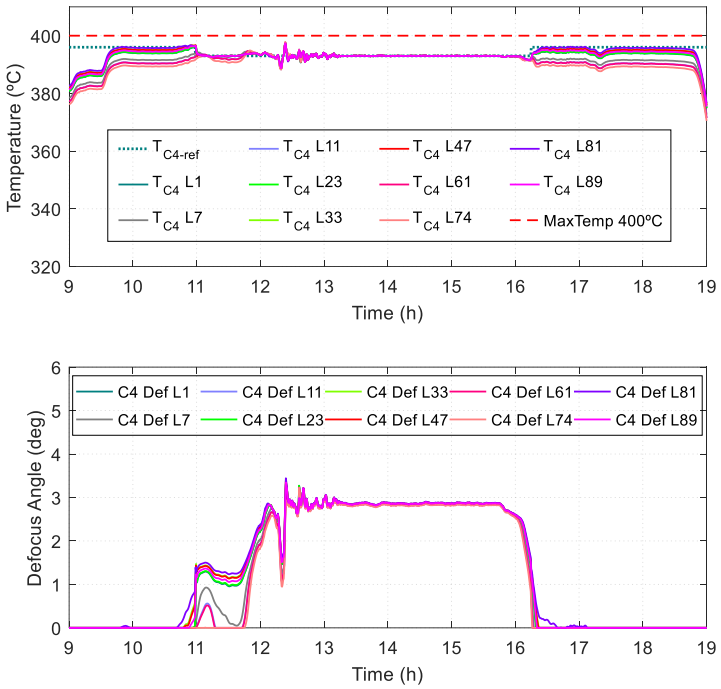

Figure 27. Flow GS-GPC + FF + C4/C3 EGS-GPC + Power EGS-GPC, 30 MW TSO limitation at 11:40am (60 min ramp) and TSO limitation off at 15:45pm (30 min ramp). Top plot: loop fluid temperatures. Bottom plot: Fourth collector defocus angle control actions.

Power tracking is presented in Figure 26. Figure 27 shows the fourth collector EGS-GPC control actions for the 10 loops and the rest of the field. It can be observed that loops have different control actions, since every loop

has different efficiency and therefore different outlet temperatures. Outlet temperatures of each loop are also within the safety limits in both situations, with and without power limitation. Figure 28 shows the third collector GS-GPC control actions of each loop. In the same way as the fourth collector, behaviour is different for each loop and for the same reason, each loop has its own controller.

Table 2. Simulated Loop Efficiencies.

Loop Number	L1	L7	L11	L23	L33
Global Efficiency	0.7776	0.7607	0.7525	0.7783	0.7865
Loop Number	L47	L61	L74	L81	L89
Global Efficiency	0.7857	0.7519	0.7445	0.7910	0.7819

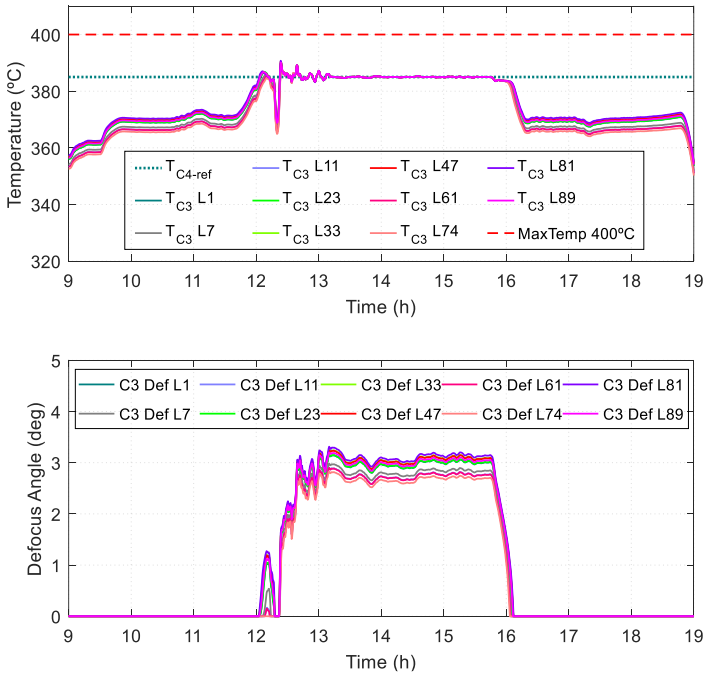

Figure 28. Flow GS-GPC + FF + C4/C3 EGS-GPC + Power EGS-GPC, 30 MW TSO limitation at 11:40am (60 min ramp) and TSO limitation off at 15:45pm (30 min ramp). Top plot: loop fluid temperatures. Bottom plot: Third collector defocus angle control actions.

4.6. Conclusion

It is reasonable to assume that the concept of optimizing a solar plant concept is directly related to terms of electric power generation. However, on some occasions, a commercial solar plant may receive a power limitation from the TSO. These commands make the plant move into an operation mode in which the objective is not maximum production. In these cases, the plant is forced to decrease its electric production and maintain the power set-point commanded by the TSO. Therefore, a problem with double objective arises: (1) temperature tracking and (2) generated power set-point tracking. The plant will have a time period to reduce its generated electric power to the set-point determined by the TSO. In this mode, the flow-rate should be decreased until the power set-point is achieved but at the cost of increasing the outlet temperature. To control the outlet temperature, secondary control is needed.

An Event-Based Gain Scheduling Generalized Predictive Control (EGS-GPC) has been presented for electric power reference tracking when power limitations appear,. In order to control the loop/field outlet temperature and to avoid exceeding oil degradation limits, an event based control strategy for defocusing the fourth and third collectors of each loop is developed with set-point changes depending on events. The linear models and control strategy have been obtained and designed by means of a 50 MW parabolic trough plant model instead of the ACUREX model. Results show the proposed MPC strategy achieves power set-points determined by the TSO in the set time periods. The Power and Defocus EGS-GPCs are capable of performing good electric power tracking and nominal set-point tracking of loop outlet temperature, avoiding oil degradation.

5. THERMAL BALANCE OF A SOLAR TROUGH FIELD

Commercial solar trough plants are of considerable size, covering vast extensions of lands. For example, the two solar trough plants at the Mojave Solar Project cover 715 hectares [5]. The SOLANA Generating Station is even larger, covering 780 hectares and it is made up of 808 solar trough loops [6]. This kind of solar plants cannot be controlled by conventional control strategies. New advanced control techniques have to be used other than those proposed in the literature.

Generally, in works developed using the ACUREX model, the efficiencies of the loops were considered equal. This is reasonable due to the small dimensions of said experimental field. However, in plants of considerable size, such as commercial ones, the efficiency of the loops can be different due to two main reasons: (1) how clean the parabolic mirrors are and (2) the deterioration of the receiver tubes, mirrors and structures. This imbalance in the optical efficiency means that the most efficient loops have to be defocused to avoid overheating problems, since in commercial plants the position of the input valves is generally configured to achieve a hydraulic balance. A preliminary work has been recently published using as a test-bench a model of the ACUREX field [19]. In this work, the input valves were manipulated to compensate the different optical efficiency of the loops. The results show that by manipulating the input valves to distribute the flow according to the optical efficiency of the loops, substantial gains can be expected. The algorithm computed the input valve opening so that the most efficient loops receive more flow-rate than the less efficient loops.

The different efficiencies of the loops is not the only disturbance affecting the thermal balance of the field. When the solar field is partially covered by clouds, the outlet temperatures of the loops can greatly vary. The control strategies proposed in the literature usually consider that the radiation measured by pyrheliometers affects the whole solar field. When the solar field is small, this assumption is reasonable, but when the solar field is large, this assumption is not reasonable [18]. Due to the size of these plants, passing clouds can cause certain groups of loops to be affected by different radiation levels to others. While some loops have a fall in temperature due to lack of radiation, others maintain an adequate temperature at their outlet. However, the temperature tracking control is

applied at the outlet temperature of the entire solar field. This temperature decreases due to the fall in temperature of the loops with little radiation. Due to this, the general HTF flow controller reduces the flow-rate to maintain the outlet temperature at its reference, 393 °C in nominal operation. The reduction of the flow-rate in the field will cause a rise in temperature of those loops with less radiation and even greater rise in those that are not covered by clouds, which will cause them to defocus so as not to degrade the HTF. The flow-rate will continue to decrease and the defocus will continue to rise until equilibrium is reached. This will lead to a loss of energy in the plant since the produced power is proportional to the flow-rate [20].

The Advanced Grant Optimal Control of solar energy systems (OCONTSOLAR), funded by the European Commission, is currently being conducted with the goal of developing new model predictive control algorithms that use mobile solar sensor estimations and predictions to yield safer and more efficient operation of plants [17]. These control strategies will use the aperture of the loop valves in order to achieve a thermal balance.

In this section, preliminary results of a nonlinear model-based optimization control algorithm to achieve an homogenization of the solar field with respect to the outlet temperature of the loops by manipulating the aperture of the inlet valves when passing clouds appear over the field, is presented. This algorithm can avoid thermal energy losses provoked by low flow-rate and/or defocus actions due to overheating problems. The algorithm is compared to the case when the input valves are not manipulated. A better thermal distribution is obtained with a reduction in thermal energy losses due to collector defocusing actions which are also reduced to a great extent.

5.1. Nonlinear Model Based Optimization for Valve Control

The objective is to obtain the optimal values of the manipulated variables, the apertures of the valves of the loops, which make the field as homogeneous as possible with respect to the outlet temperature of the loops

in steady state and, therefore, avoids thermal energy losses by flow-rate and/or defocus.

The optimization algorithm minimizes a cost function subject to constraints in order to obtain the closest temperature to a reference as formulated in (16).

$$\begin{aligned} minJ \quad & = \sum_{n=1}^{NLoop} \left(\sum_{j=N_1}^{N_2} \delta(j)[\hat{y}_n(t+j|t) - w(t+j)]^2 \right. \\ & \left. + \sum_{j=1}^{N_u} \lambda(j)[\Delta u_n(t+j-1)]^2 \right) \\ s.t: & \\ & U_{min} < U(t+j) < U_{max} \\ & \Delta u_{min} < \Delta u(t+j) < \Delta u_{max} \\ & x = f(x,U), y = g(x) \end{aligned} \tag{16}$$

However, since the flow controller may be acting on disturbances or on reference changes, among others, the objective function will try to minimize the distance between the outlet temperatures of loops instead of bringing it closer to a set-point. In this way, the solar field will be homogenized when it reaches the steady state.

To solve the problem, the non-linear distributed parameter model is used, which must be iterated along a prediction horizon. In this case, weighting the control and output signal is not needed in the cost function as the valves are not being controlled along a control horizon. The prediction horizon is used to obtain the simulated prediction and perform the optimization, but the objective is not a temperature set-point tracking problem minimizing the movement of the valves but to calculate only one control signal for each valve to homogenize the field.

Since only one value for each manipulated variables is going to be obtained, control increment constraints are not included in the problem formulation. The only constraint taken into account for this optimization is the maximum and minimum aperture, $U_{min} < U(t+j) < U_{max}$. Since the objective is to control the valves in this way in steady state a homogenization of the field temperatures is achieved, it is not necessary to include all the steps along the prediction horizon in the cost function. Although it continues using the complete horizon to simulate the system in order to obtain the

optimal solution, the cost function only contemplates the temperature at the end of the horizon. In this way the complexity of the problem is reduced by simplifying the cost function. The proposed cost function is described in (17).

$$\begin{aligned} minJ \quad & = min \sum_{m=1}^{N_{Loop}} \sum_{n=1}^{N_{Loop}} |\hat{y}_m(N_2) - \hat{y}_n(N_2)| \\ s.t: \quad & \\ & U_{min} < U(t+j) < U_{max} \\ & x = f(x,U), y = g(x) \end{aligned} \tag{17}$$

Nonlinear valve control (NLVC) does not change the flow-rate of the plant but receives it as an input, so that there is no direct interaction with the flow-rate controller which is controlling the field outlet temperature. In fact, it is important that it does not have direct interaction to avoid coupling or resonant modes in the plant. The optimization problem is computed every 5 minutes in order to be able to track the transients and to have the field as homogenized as possible.

5.2. Simulated Plant Scenario

The simulated plant consists of two fields of 45 loops each (90 loops) with its power block in the center, see Figure 1. The simulation performed consists of a series of clouds that partially cover the upper field while the lower field is not be affected by these radiation transients.

A mild summer day with a medium level of radiation is simulated to show the results of valve control using the explained optimization algorithm. A series of clouds will pass over the solar field, partially covering different parts. It is considered that the clouds enter from the west and moves towards the east. Likewise, the clouds only affects the upper field and various collectors of the solar field. In one case, clouds affect collectors 2 and 3, leaving collectors 1 and 4 with full radiation. In another case, collectors 1 and 4 are affected. The clouds have been generated irregularly and are presented in Figure 29 in radiation captures at different instants in time.

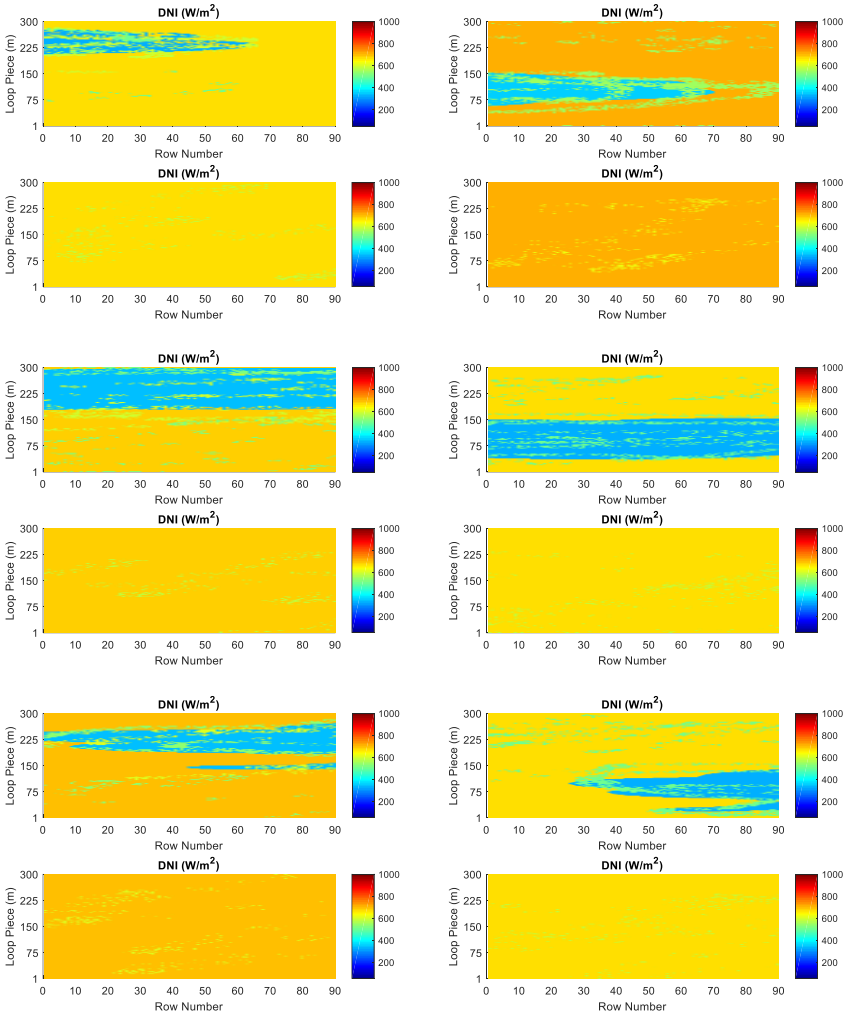

Figure 29. Partial coverage of the solar field by passing clouds.

Although the 50 MW plant has 90 loops, consideration that clouds enter from the west, the simulation has been carried out in blocks of 9 loops. In this way, the optimization consists of 10 manipulated variables (group valves). These blocks have been assumed for two reasons: (1) radiation can be assumed similar in small portions of the solar field and (2) an adequate

calculation must be obtained within the proposed sampling time. The blocks have been called B1-B10, with B1-B5 being the blocks of the upper field and B6-B10 those of the lower field. The use of loop groups is done to relax the problem and reduce the computation time of the nonlinear optimization.

As mentioned above, the OCONTSOLAR project will use techniques for collecting data through the use of drone fleets. The objective of these fleets is to create a radiation map of the plant in the areas of greatest interest. To show the results expected to be obtained through the control of valves and the radiation data sent by the drone fleet, the radiation map is assumed to be known.

In this scenario, the flow-rate and defocus controllers of the previous section will be applied. The temperature set-point for the flow-rate controller is set to 393 °C (nominal temperature). In this simulation, only fourth collector defocus control is applied. The temperature set-point for the fourth collector is fixed at 395 °C. Since the third collector is not needed when there is no power limitation, applying only the fourth collector defocus control is used.

5.3. Simulation Results

In Figures 30, 31, 32 and 33 the results of the simulations, both when no valve control is applied and when the proposed NLVC is applied, are shown.

Figure 30 shows the temperatures of the fluid in the different blocks for the simulations when no valve control is applied and for when the NLVC is applied, in order to compare the benefit of a field thermal balance by means of controlling the inlet valves.

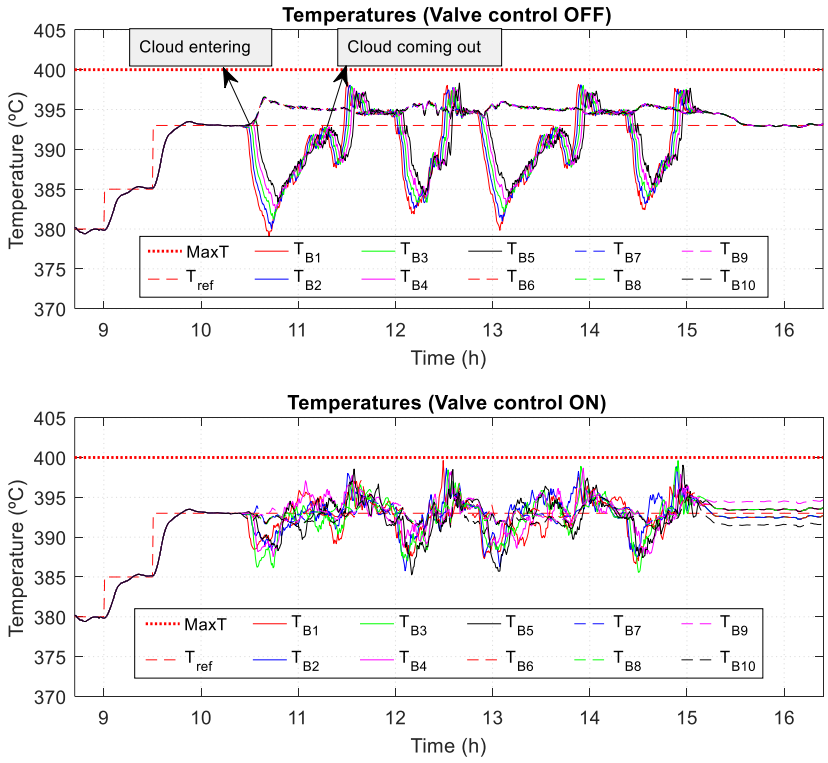

Figure 30. Loops temperatures. Top plot: Loop blocks outlet temperatures, no valve control. Bottom plot: Loop blocks outlet temperatures, NLVC.

It can be observed how the temperatures of the upper field decrease as the clouds partially cover the field. In the same way, the temperatures of the loops of the lower field increase until they have to be controlled by the defocus control of the loops. Four transients can be observed throughout the simulation. These transients are partially covering the field. In some cases they cover collectors 2 and 3, and in others, collectors 1 and 4.

The great difference between the temperatures of the different loops is easily appreciable. Applying valve control through the proposed NLVC, it is easy to check how the temperatures of the loops are confined to a much smaller range.

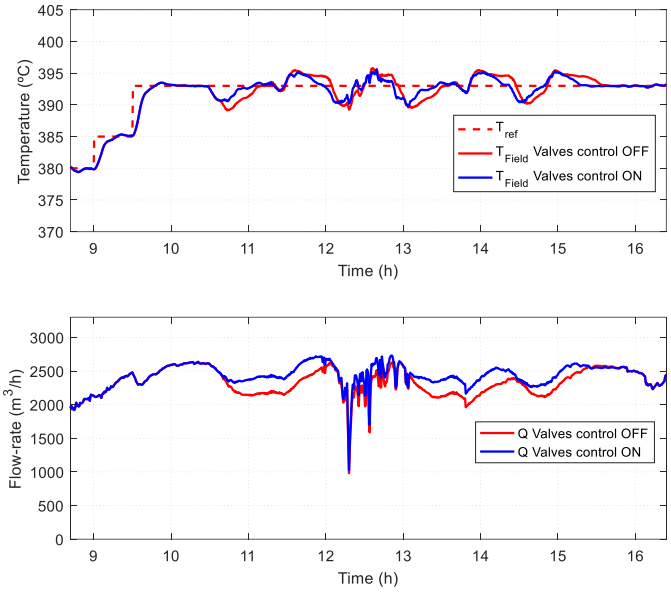

Figure 31. Field state. Top plot: Field outlet temperature. Bottom plot: Field flow-rate.

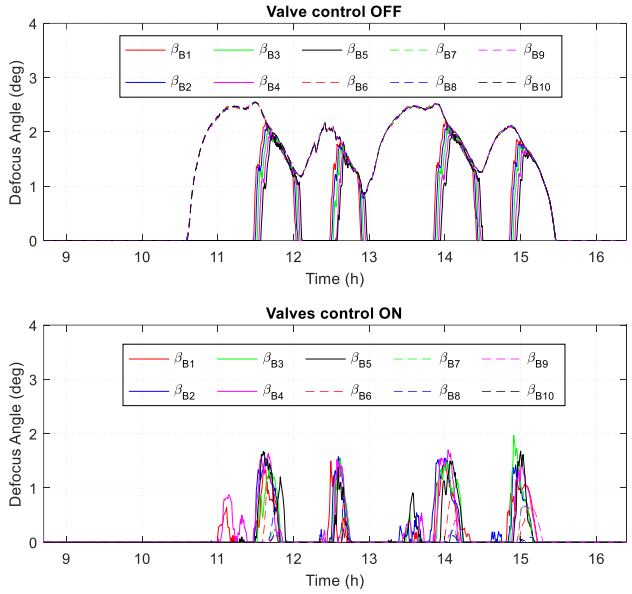

Figure 32. Loop defocusing angles comparison. Top plot: Loop blocks defocusing actions, no valve control. Bottom plot: Loop block defocusing actions, NLVC.

In Figure 31 the field outlet temperature and the flow-rate of both simulations are presented. The valve control strategy is able to maintain the outlet temperature in a range closer to the desired set-point. The flow-rate circulating through the field is greater when acting on the valves to homogenize the field. The proposed strategy is able to maintain a higher level of flow-rate at the same field temperature, which means, more output power.

The results of the defocus are clearly diminishes when acting on the valves, see Figure 32, since the flow-rate in the cloud-free loops is greater and the field is more balanced and smaller defocus actions are needed. Tables 3 and 4. show the average reduction in the number of defocus actions that has to be applied in both scenarios and the average reduction in the total travelled angle of the collectors.

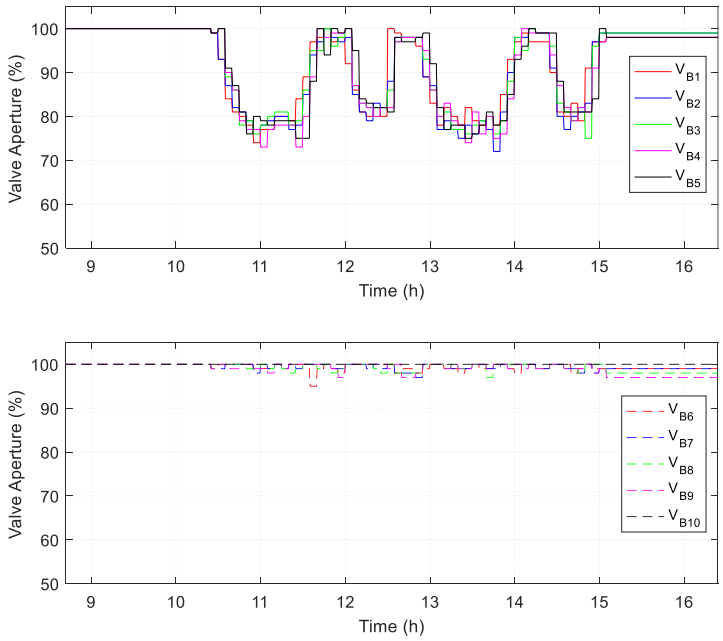

Figure 33. NLVC valve control actions. Top plot: Loop blocks B1-B5 (upper field) valve apertures. Bottom plot: Loop blocks B6-B10 (lower field) valve apertures.

Figure 33 shows the control actions on the valves. It can be seen how the valves are modified as the irradiation on the field is affected by clouds, see Figure 30.

Table 3. Defocus Reduction (10am - 16pm)

Block Number	Average defocus actions (no control)	Average defocus actions (valve control)	Reduction (%)
1	256	211	-17.5781
2	253	221	-12.6482
3	247	172	-30.3644
4	242	231	-4.5455
5	241	184	-23.6515
6	585	96	-83.5897
7	585	81	-86.1538
8	585	75	-87.1795
9	585	107	-81.7094
10	585	48	-91.7949

Table 4. Travelled Angles Reduction (10am - 16pm)

Block Number	Average defocus actions (no control)	Average defocus actions (valve control)	Reduction (%)
1	18.8667	18.4810	-2.0443
2	19.1393	20.2184	5.6382
3	18.9969	18.1943	-4.2252
4	17.6064	22.3358	26.8616
5	17.6424	20.0369	13.5726
6	14.6783	7.0029	-52.2907
7	15.0485	4.1660	-72.3163
8	15.0323	3.8613	-74.3132
9	15.1356	3.9137	-74.1427
10	14.9211	1.3834	-90.7285

As previously mentioned, the effect of defocusing and flow-rate may entail a loss of energy when high outlet temperatures are desired. Table 5 shows the results of the average electric power (MW) generated in the two simulations from 10:00 to 16:00 hours. The results show an improvement of 6.5% when applying the NLVC.

Table 5. Power (MW) Improvement (10am - 16pm)

Mean Power Valves OFF	Mean Power Valves ON	Improvement (%)
38.0006	40.4707	6.5

By applying valve control on the solar field for rejecting disturbances such as passing clouds several objectives can be achieved:

1. Thermal balance of the solar field reducing the temperature gradients between the different loops. This is especially interesting in commercial plants given that temperature gradients are not only detrimental to the state of the receiver tubes but also beneficial for a more homogeneous mixing of loop temperatures in the outlet manifold.
2. Smaller number of defocusing actions due to the homogenization of the solar field, extending the life of the actuators.
3. When high process temperatures are required, such as the nominal one, power losses can be avoided due to the flow-rate reduction to maintain the outlet temperature.

5.4. Conclusion

In this section, within the framework of the OCONTSOLAR project, a preliminary study has been presented regarding a nonlinear valve control model based strategy (NLVC) to deal with the loss of electrical power due to clouds that partially cover the solar field. The results show that by not applying adequate control over the valves and using the flow-rate and the defocus to control the field lead to energy losses as well as large variations amongts the temperatures of the loops. The proposed NLVC strategy shows that it is possible to avoid energy losses in partial transients due to a decrease in flow-rate and defocusing the hottest loops. The homogeni-zation of field temperatures leads to a higher flow-rate and less defocus actions on the loops. Applying the proposed strategy provides a considerable improvement

of up to 6% in the average electrical power generated when high temperatures at the outlet are needed.

ACKNOWLEDGEMENTS

The authors would like to acknowledge the European Research Council (ERC) for funding this work under the European Union's Horizon 2020 research and innovation programme (advanced grant OCONTSOLAR, grant agreement No 789051).

REFERENCES

[1] Goswami, D., Kreith, F. and Kreider, J. (2000). *Principles of Solar Engineering.* (2th ed.). Taylor & Francis.

[2] Craig, O. O., Brent, A. C. and Dinter, F. (2017). The current and future energy economics of concentrating solar power (csp) in south africa. *South African Journal of Industrial Engineering* 28(3), 1–14.

[3] Atlantica Yield (2018). http://www.atlanticayield.com/. (accessed May 1, 2019).

[4] Power Technology (2019). *The Andasol Solar Power Station Project.* https://www.power-technology.com/projects/andasolsol arpower/. (accessed May 1, 2019).

[5] National Renewable Energy Laboratory (NREL) (2015a). Concentrating Solar Power Projects. *Mojave Solar Project.* https://solarpaces.nrel.gov/mojave-solar-project. (accessed May 1, 2019).

[6] National Renewable Energy Laboratory (NREL) (2015b). Concentrating Solar Power Projects. *Solana Generating Station.* https://solarpaces.nrel.gov/solana-generating-station. (Accessed May 1, 2019).

[7] N.A Engineering (2008). National Academy of Engineering. *Grand challenges for engineering.* www.engineeringchallenges.org. (Accessed May 1, 2019).

[8] European Commission (2015). *Communication of the Commission to the European Parliament and the Council concerning the Paris Protocol-A blueprint for tackling global climate change beyond 2020.* https://ec.europa.eu/commission/publications/paris-protocol blueprint-tackling-global-climate-change-beyond-2020en. (Accessed May 1, 2019).

[9] Camacho, E. F. and Gallego, A. J. (2013). Optimal operation in solar trough plants: A case study. *Solar Energy* 95, 106 – 117.

[10] Berenguel, M., Cirre, C. M., Klempous, R., Maciejewski, H., Nikodem, M., Nikodem, J., Rudas, I. and Valenzuela, L. (2005). Hierarchical control of a distributed solar collector field. In *Computer Aided Systems Theory*. EUROCAST 2005, pp. 614–620.

[11] Camacho, E. F., Rubio, F. R., Berenguel, M. and Valenzuela, L. (2007). A survey on control schemes for distributed solar collector fields. part ii: Advanced control approaches. *Solar Energy* 81(10), 1252 – 1272.

[12] Camacho, E. F., Soria, M. B., Rubio, F. R. and Martínez, D. (2012). *Control of Solar Energy Systems* (1st ed.). Springer-Verlag London.

[13] Lemos, J. M., Neves-Silva, R. and Igreja, J. M. (2014). *Adaptive Control of Solar Energy Collector Systems.* Springer-Verlag.

[14] Gil, P., Henriques, J., Cardoso, A., Carvalho, P. and Dourado, A. (2014, March). Affine neural network-based predictive control applied to a distributed solar collector field. *IEEE Transactions on Control Systems Technology* 22(2), 585–596.

[15] Camacho, E. F. and Gallego, A. J. (2015). Model predictive control in solar trough plants: A review. In *5th IFAC Conference on Nonlinear MPC,* September 17-20, Sevilla (Spain).

[16] Power Technology (2015). *Mojave Solar Thermal Power Facility*, San Bernardino County, California. https://www.powertechnology. com/projects/mojave-solar-thermal-power- california-us/.

[17] European Commission (2018). *Community Research and Development Information Service OCONTSOLAR.* https://cordis.europa.eu/project/rcn/216250 es.html. (Accessed May 1, 2019).

[18] Gallego, A. J. and Camacho, E. F. (2012). Adaptative state-space model predictive control of a parabolic-trough field. *Control Engineering Practice* 20(9), 904 – 911.

[19] Sánchez, A. J., Gallego, A. J., Escaño, J. M. and Camacho, E. F. (2018a, May). Temperature homogenization of a solar trough field for performance improvement. *Solar Energy*. 165C, 1–9.

[20] Sánchez, A. J., Gallego, A. J., Escaño, J. M. and Camacho, E. F. (2018b, November). Event-based mpc for defocusing and power production of a parabolic trough plant under power limitation. S*olar Energy* 174, 570 –581.

[21] Sánchez, A. J., Gallego, A. J., Escaño, J. M. and Camacho, E. F. (2019 May). Adaptive incremental state space mpc for collector defocusing of a parabolic trough plant. *Solar Energy* 184, 105–114.

[22] National Renewable Energy Laboratory (NREL) (2013). *Concentrating Solar Power Projects.* Helios I. https://solarpaces.nrel.gov/helios-i. (Accessed May 1, 2019).

[23] National Renewable Energy Laboratory (NREL) (2017a). *Concentrating Solar Power Projects.* Guzmán. https://solarpaces.nrel.gov/guzman. (Accessed May 1, 2019).

[24] National Renewable Energy Laboratory (NREL) (2017b). *Concentrating Solar Power Projects.* Ibersol Ciudad Real (Puertollano). https://solarpaces.nrel.gov/ibersol-ciudad-real-puertollano. (Accessed May 1, 2019).

[25] National Renewable Energy Laboratory (NREL) (2017c). *Concentrating Solar Power Projects.* Extresol 1. https://solarpaces.nrel.gov/extresol-1. (Accessed May 1, 2019).

[26] National Renewable Energy Laboratory (NREL) (2017d). *Concentrating Solar Power Projects*. Solaben 2. https://solarpaces.nrel.gov/solaben-2. (Accessed May 1, 2019).

[27] Carmona, R. (1985). *Analisis, modelado y control de un campo de colectores solares distribuidos con sistema de seguimiento en un eje.*

Ph.D. Thesis. Universidad de Sevilla. [*Analysis, modeling and control of a distributed solar collector field with tracking system on one axis.* Ph.D. Thesis. University of Seville].

[28] Camacho, E. F., Berenguel, M. and Rubio, F. R. (1997). *Advanced Control of Solar Plants*. Springer Science & Business Media.

[29] National Renewable Energy Laboratory (NREL) (2017). Concentrating Solar Power Projects. *Majadas I.* https://solarpaces.nrel.gov/majadasi. (Accessed May 1, 2019).

[30] National Renewable Energy Laboratory (NREL) (2013). *Concentrating Solar Power Projects.* Palma del Río I. https://solarpaces.nrel.gov/palma-del-rio-i. (Accessed May 1, 2019).

[31] Rohani, S., Fluri, T., Dinter, F. and Nitz, P. (2017). Modelling and simulation of parabolic trough plants based on real operating data. *Solar Energy* 158, 845 – 860.

[32] National Renewable Energy Laboratory (NREL) (2017a). *Concentrating Solar Power Projects.* Andasol 1. https://solarpaces.nrel.gov/andasol-1. (Accessed May 1, 2019).

[33] National Renewable Energy Laboratory (NREL) (2017b). *System Advisor Model (SAM).* https://sam.nrel.gov/. (Accessed May 1, 2019).

[34] Geyer, M., Lüpfert, E., Osuna, R., Esteban, A., Schiel, W., Schweitzer, A., Zarza, E., Nava, P., Langenkamp, J. and Mandelberg E. (2002, September). Eurotrough - parabolic trough collector developed for cost efficient solar power generation. In *11th SolarPACES International Symposium on Concentrated Solar Power and Chemical Energy Technologies.*

[35] Kearney, D. W. (2007). *Parabolic trough collector overview*. Parabolic trough workshop, NREL.

[36] Lüpfert, E., Zarza, E., Schiel, W., Osuna, R., Esteban, A., Geyer, M., Nava, P., Langenkamp, J., Mandelberg, E. (2003). *EUROTROUGH Collector Qualification complete-performance test results from PSA.* In: Proceedings of ISES Solar World Congress, 14–19 June 2003, Göteborg, Sweden.

[37] SCHOTT Solar CSP GmbH (2019). *SCHOTT PTRR 70 Receivers.* https://www.us.schott.com/csp/english/schott-solar-ptr-70-receivers.html. (Accessed May 1, 2019).

[38] Eastman Chemical Company (2019). *Therminol VP-1 Heat Transfer Fluid.* https://www.therminol.com/products/Therminol-VP1. (Accessed May 1, 2019).

[39] Schenk, H., Dersch, J., Hirsch, T. and Polklas, T. (2015, September). Transient simulation of the power block in a parabolic trough power plant. In *The 11th International Modelica Conference Versailles, France*, pp. 605–614. Linköping University Electronic Press, Linköpings universitet.

[40] Montañés, R. M., Windahl, J., Palsson, J. and Thern, M. (2018). Dynamic modeling of a parabolic trough solar thermal power plant with thermal storage using modelica. *Heat Transfer Engineering* 39(3), 277–292.

[41] Burkholder, F., Brandemuehl, M., Price, H., Netter, J., Kutscher, C. and Wolfrum, E. (2007). Parabolic trough receiver thermal testing. In *Energy Sustainability, ASME 2007 Energy Sustainability Conference*, pp. 961–970.

[42] Lüpfert, E., Riffelmann, K., Price, H., Burkholder, F. and Moss, T. (2008, May). Experimental analysis of overall thermal properties of parabolic trough receivers. *Journal of Solar Energy Engineering* 130(2).

[43] Camacho, E. F. and Bordons, C. (2007). *Model Predictive control* (2th ed.). Springer-Verlag London.

[44] Camacho, E. F., Berenguel, M. and Rubio, F. R. (1994). Application of a gain scheduling generalized predictive controller to a solar power plant. *Control Engineering Practice* 2(2), 227–238.

[45] Camacho, E. F., Rubio, F. R. and Hughes, F. M. (1992, April). Selftuning control of a solar power plant with a distributed collector field. *IEEE Control Systems* 12(2), 72–78.